Characterization of ANGPT2 mutations associated with primary lymphedema

Leppänen, Veli-Matti

2020-09-09

Characterization of *ANGPT2* mutations associated with primary lymphedema

Authors: Veli-Matti Leppänen[1,2,*], Pascal Brouillard[3,*], Emilia A Korhonen[1], Tuomas Sipilä[1],

Sawan Kumar Jha[2], Nicole Revencu[4], Veerle Labarque[5], Elodie Fastré[3], Matthieu Schlögel[3],

Marie Ravoet[4], Amihood Singer[6], Claudia Luzzatto[7], Donatella Angelone[8], Giovanni Crichiutti[9],

Angela D'Elia[9], Jaakko Kuurne[1], Harri Elamaa[10], Gou Young Koh[11, 12], Pipsa Saharinen[1,2],

Miikka Vikkula[3,13,†,‡] and Kari Alitalo[1,2,†,‡]

[1] Wihuri Research Institute, Biomedicum Helsinki, Haartmaninkatu 8, 00290 Helsinki, Finland

[2] Translational Cancer Medicine Program, Faculty of Medicine and Helsinki Institute of Life

Science, 00014 University of Helsinki, Finland

[3] Human Molecular Genetics, de Duve Institute, University of Louvain, 1200 Brussels, Belgium

[4] Center for Human Genetics, Cliniques universitaires Saint-Luc, University of Louvain, 1200

Brussels, Belgium

[5] Centre for Molecular and Vascular Biology, University of Leuven, 3000 Leuven, Belgium

[6] Barzilai Medical Center, 78306 Ashekelon, Israel

[7] Padova University Hospital, 35128 Padova, Italy

[8] A. Gemelli Hospital, 00168 Roma, Italy

[9] Azienda Ospedaliero-Universitaria Santa Maria della Misericordia, 33100 Udine, Italy

[10] Oulu Centre for Cell-Matrix Research, Faculty of Biochemistry and Molecular Medicine,

Biocenter Oulu, 90220 University of Oulu, Finland

[11] Center for Vascular Research, Institute of Basic Science, and

[12] Graduate School of Medical Science and Engineering, Korea Advanced Institute of Science

and Technology (KAIST), 34141 Daejeon, Republic of Korea.

[13] Walloon Excellence in Lifesciences and Biotechnology (WELBIO), University of Louvain,

1200 Brussels, Belgium

*V.-M. Leppänen and P. Brouillard contributed equally to this work.

†M. Vikkula and K. Alitalo contributed equally to this work.

‡Corresponding author. Email: miikka.vikkula@uclouvain.be and kari.alitalo@helsinki.fi

Overline: VASCULAR BIOLOGY

One Sentence Summary

Loss-of-function mutations in the TIE2-ligand angiopoietin 2 are associated with primary lymphedema in humans.

Abstract

Primary lymphedema is caused by developmental and functional defects of the lymphatic vascular system that result in accumulation of protein-rich fluid in tissues, causing edema. The 28 currently known genes causing lymphedema explain <30% of cases. Angiopoietin 1 (ANGPT1) and ANGPT2 function via the TIE1-TIE2 (Tyrosine kinase with Immunoglobulin-like and EGF-like domains 1 and 2) receptor complex and α5β1 integrin to form an endothelial cell (EC) signaling pathway that is critical for blood and lymphatic vessel formation and remodeling during embryonic development, as well as for homeostasis of the mature vasculature. By screening a cohort of 543 individuals affected by primary lymphedema, we identified one heterozygous de novo *ANGPT2* whole-gene deletion and four heterozygous *ANGPT2* missense mutations. Functional analyses revealed three missense mutations that resulted in decreased ANGPT2 secretion and inhibited the secretion of wild-type (WT)-ANGPT2, suggesting that they have a dominant-negative effect on ANGPT2 signaling. The WT-ANGPT2 and soluble mutants T299M and N304K activated TIE1 and TIE2 in an autocrine assay in human lymphatic endothelial cells. Molecular modeling and biophysical studies showed that N-terminally truncated ANGPT subunits formed asymmetrical homodimers that bound TIE2 in a 2:1 ratio. The T299M mutant, located in the dimerization interphase, showed reduced integrin-α5 binding and its expression in mouse skin promoted hyperplasia and dilation of cutaneous lymphatic vessels. These results show that primary lymphedema can be associated with *ANGPT2* mutations, and provide insights into TIE1 and TIE2 activation mechanisms.

Introduction

Lymphedema manifests as tissue swelling and results from defective drainage of lymphatic fluid from the interstitial tissue due to impaired lymphatic development or function. Primary lymphedema is a rare condition with autosomal dominant inheritance, which was initially characterized by mutations in the vascular endothelial growth factor receptor 3 (VEGFR-3) gene *FLT4* (*1-3*). Germline mutations responsible for various types of primary lymphedema have since been identified in 28 genes that encode proteins involved mainly in VEGFR-3 signaling, including transcription factors such as GATA2, FOXC2, and SOX18 (*4, 5*). The mutant alleles usually cause reduced activity of the VEGFR-3 pathway (*5, 6*). These genes explain less than 30% of primary lymphedema cases, necessitating a search for additional lymphedema-associated genetic defects.

The angiopoietin-TIE receptor tyrosine kinase signaling pathway is necessary for blood and lymphatic vessel remodeling during embryonic and postnatal development, and for homeostasis of the mature vasculature (*7, 8*). Angiopoietins (ANGPTs) have a modular structure consisting of an N-terminal super clustering domain, a coiled-coil region and a C-terminal fibrinogen-like domain (*9*) that is involved in TIE2 binding. ANGPT1 is secreted by perivascular cells and acts in a paracrine manner (*10, 11*). A second autocrine ligand, ANGPT2, is synthesized, stored and secreted by ECs (*12, 13*). ANGPT2 was originally considered a naturally occurring antagonist of ANGPT1 as it can compete with ANGPT1 for binding to TIE2, thereby decreasing TIE2 phosphorylation in vascular ECs (*14*). However, at least in adult tissues, ANGPT2 can also act as a weak agonist to promote vascular remodeling (*15*). Additionally, transgenic overexpression of Angpt2 in mice results in embryonic lethality because of vascular defects similar to Angpt1-null mice (*14*). Furthermore, ANGPT2 is selectively expressed in ECs of actively remodeling vessels, for example in tumors (*16*), and contributes to endothelial destabilization in inflammation and cancer (*17*).

Angpt2-deficient mice and Angpt2 antibody-based targeting have shown that Angpt2 acts as a TIE2 agonist in lymphangiogenesis (*18-22*). Embryos with homozygous deletion of the *Angpt2* gene or treated with ANGPT2-blocking antibodies have abnormal, defective lymphatic vessels (*18-20*). The major co-receptor that modulates TIE2 signaling is TIE1 (*15, 23*). Both Tie1 and Tie2 are

4

required for development of lymphatic valves and collecting vessels in mice, providing a mechanism of Angpt2-mediated lymphangiogenesis (*21, 24-27*). Lymphatic ECs (LECs) express only low amounts of the EC-specific protein tyrosine phosphatase VE-PTP that associates with TIE2 and TIE1 and downregulates their phosphorylation (*27, 28*). This increases ANGPT2 agonistic activity towards TIE2 in LECs. Angiopoietins also interact with the EC-specific integrins α5β1 and αvβ3 that modulate TIE2 signaling, and ANGPT2 activates α5β1-integrin signaling in ECs when TIE2 expression is decreased (*15, 17, 29-32*).

Genetic variants in the ANGPT-TIE2 pathway have been associated with several diseases. Inherited gain-of-function and loss-of-function mutations in the TIE2 gene *TEK* underlie inherited venous malformations (VMCM) and primary congenital glaucoma, respectively (*33, 34*). Somatic gain-of-function TIE2 mutations are associated with sporadic venous malformations, multifocal sporadic venous malformations and the Blue Rubber Bleb nevus syndrome (*35, 36*). *ANGPT1* variants were linked to hereditary angioedema in one family and to primary congenital glaucoma in two other families (*37, 38*). In addition, *ANGPT2* gene polymorphisms were associated with altered plasma ANGPT2 isoform ratios and predisposition to acute lung injury after trauma (*39*).

Here, we describe mutations in the *ANGPT2* gene identified in a cohort of 543 patients with primary lymphedema and investigate how these mutations alter ANGPT2 structure and function. Our data underscore loss of ANGPT2 function as a mechanism leading to primary lymphedema.

Results

Identification of five *ANGPT2* mutations in patients with primary lymphedema

We explored a cohort of 543 index patients with primary lymphedema for mutations in the 28 known lymphedema genes as well as candidate lymphedema-causing genes selected from the literature based on their function in the lymphatic system. Among patients with no mutations in the known genes, we observed a complete *ANGPT2* gene deletion in one family, and identified four variants of interest in *ANGPT2* in four other families (Fig. 1, A and B). These variants were extremely rare (<0.02%) or absent in the Genome Aggregation Database (gnomAD) population database, and they were predicted to be pathogenic by several prediction software tools. According

to gnomAD, the probability of the *ANGPT2* gene to be LOF-intolerant was high (pLI=0.83; range 0.00 to 1.00) with an observed/expected ratio of 0.38. This implies that LOF variants are negatively-selected in the general population, yet some are tolerated, potentially due to the reduced penetrance commonly seen in lymphedema-causing genes (*40*).

Family LE-851 (Belgian). This patient (boy) was noticed to have bilateral lower extremity lymphedema up to the knees at around 8-9 weeks of age. He had temporary thrombocytopenia but no other associated signs or symptoms and his management (at the age of 1.5 years) was based on follow-up. His parents had no signs of lymphedema (Fig. 1, A and B). He had a heterozygous deletion encompassing all *ANGPT2* exons. The deletion was not present in either parent.

Family LE-128 (Italian). This patient (girl) presented at 6 months with lymphedema of the right leg, below the knee (Fig. 1, A, B and C), and episodes of cellulitis. She developed lymphatic vesicles in the great labia around age twelve that were repeatedly treated with laser. She wears contention stockings and, in the summer, uses a pneumatic compression device. Her father (48 y.o. at the time of this writing) developed lymphedema at eight years, initially confined to the right foot and ankle. At twelve, he had surgery for bilateral hydrocele, and later developed edema and swelling of the scrotum and penis with worsening phologose and fluid leakage. At the age of 33 and 35 years, he had surgeries to reduce scrotal dimensions. He subsequently developed lymphedema of the right thigh (Fig. 1D). He has been treated twice for cellulitis. Lymphoscintigraphy in at the age of 47 years (Fig. 1D) showed several inguinal-crural nodes on the left side after 20 min, and lymphatic vessels at 60 min. On the right (affected) side, only skin diffusion at the distal part was observed after 20 min, and after 60 min a single dilated vessel was visualized with no activity in the inguinal-crural nodes. Evidence of iliac nodes was observed. In a deeper scan, good visualization of one lymphatic vessel and some inguinal-crural nodes was observed on the left side after 60 min, with no detectable activity on the right side. The patient's brother, sister, and mother were unaffected. The index patient and her father had a heterozygous nucleotide change (c.896C>T) in *ANGPT2*, which corresponds to Thr299 substitution by a methionine (Fig. 1, A and B). This variant was predicted to be damaging by Polyphen2, LRT, Mutation Taster, and Mutation Assessor.

Family LE-65 (Israeli). The patient was born at 25 weeks of gestation from healthy parents. He had bilateral lower-leg lymphedema and hydrocele. The patient and his unaffected father had a heterozygous nucleotide substitution (c.912T>A) in *ANGPT2* corresponding to Asn304 substitution by a lysine (Fig. 1, A and B), which was predicted as damaging to ANGPT2 function by SIFT, LRT, Mutation Taster, and Polyphen2.

Family LE-148 (Italian). This patient displayed increased nuchal translucency during gestation. At birth, he had congenital lymphedema of the feet (Fig. 1E) and left hand, and an abdomino-scrotal hydrocele. The lymphedema gradually resorbed, but was still present. He had surgery for hydrocele at three years of age. He had no other health issues. His father (LE-148-100) also had congenital lymphedema involving the lower legs and feet, both arms and hands, and neck. His lymphedema spontaneously resorbed. Lymphedema of the feet and varicose veins were also reported for the paternal grandfather, whose DNA was not available for testing. The mother, the grand-mother and the paternal uncle were asymptomatic. We identified a heterozygous nucleotide substitution (c.1304G>C) in *ANGPT2* in both the index patient and his father (Fig. 1, A and B). The mutation resulted in a substitution of Cys435 by serine, and was predicted to impact ANGPT2 function by LRT, Mutation Taster, Polyphen2 and CADD.

Family LE-623 (Italian). This girl developed bilateral lymphedema below the ankles after birth, accompanied with facial dysmorphism, epicanthus, low-implanted ears, upslanted palpebral fissures, thin upper lip, microcephaly, epilepsy, and developmental delay. Her parents were asymptomatic. The index patient and her unaffected mother (Fig. 1, A and B) had a heterozygous nucleotide substitution (c.1475G>A) in *ANGPT2* corresponding to an Arg492 substitution by glutamine. This mutation was predicted to alter the function by SIFT, LRT, Mutation Assessor, Mutation Taster, Polyphen2, and CADD.

Structural characterization of ANGPT2 mutations

All of the identified *ANGPT2* substitutions were located in the fibrinogen-like domain, which is responsible for ANGPT2 binding to TIE2 (Fig. 2, A and B). However, analysis of the T299M, N304K, C435S and R492Q substitutions in the structure of the WT-ANGPT2-TIE2 complex (PDB code 2GY7) indicated that the substituted residues were not directly involved in TIE2 binding (Fig.

2B). The Thr299 and Asn304 residues are located on the surface of the protein and the replacement of these residues did not seem to induce unfavorable interactions in the monomeric ANGPT2 fibrinogen-like domain (fig S1, A and B). Notably, Asn304 occurs in a N-glycosylation consensus sequence NXT (Asn304-Ser305-Thr306), suggesting that its mutation may lead to altered glycosylation. The third ANGPT2 mutation occurred at Cys435, which is disulfide-bonded with Cys450 in WT-ANGPT2 (fig. S1C). The C435S mutation would not allow the formation of this disulfide bridge, thus destabilizing the corresponding ANGPT2 loop, which is involved in TIE2 binding. Arg492 and the neighboring residues make multiple hydrogen bonds and salt bridges, which are lost upon the R492Q mutation. Gln492 in the position of Arg492 was also predicted to make unfavorable polar and nonpolar van der Waals interactions and result in steric clashes (fig. S1D).

Expression of ANGPT2 mutants

To test the effects of the mutations on protein expression and secretion, we transfected WT and mutant ANGPT2 expression vectors into HEK293 cells and analyzed the cell lysates and culture media for ANGPT2 protein by western blotting and ELISA assays (Fig. 2, *C* and *D*). We observed a large difference between mobilities of the intracellular and secreted ANGPT2 polypeptides, indicating that ANGPT2 maturation involves extensive post-translational modification. Both WT and mutant ANGPT2 polypeptides were detected in the lysates, but the C435S and R492Q mutants were not detected in the supernatants and the amount of the N304K polypeptide was lower than that of the WT protein. ELISA confirmed that the concentration of the ANGPT2 T299M mutant was comparable to that of WT-ANGPT2, whereas the C435S mutant was undetectable and R492Q mutant was barely detectable. Of interest, the concentration of ANGPT2 in the EDTA-plasma from patient LE-623-10, heterozygous for the R492Q mutation, was lower (1220 pg/ml) than in unaffected controls (mean=1960 pg/ml; n=3). ANGPT2 N304K protein concentrations in the supernatants were also decreased and had an increased mobility in gel electrophoresis (Fig. 2C and fig. S2A), confirming that the Asn304 glycosylation site was lost in this mutant.

Because all the mutations found in patients were heterozygous, we also analyzed the effect of the mutant proteins on expression of WT-ANGPT2. We co-transfected expression vectors encoding WT-ANGPT2 and the C435S or R492Q mutant into HEK293 cells. Both mutants reduced the total

ANGPT2 secreted into the culture medium (Fig. 2E), suggesting that they make heteromers with WT-ANGPT2, thereby affecting its secretion or folding. Although the C435S mutant had the lowest expression when transfected alone, the reduction of total soluble ANGPT2 was significantly greater ($P = 0.04$) upon co-transfection with the R492Q mutant than with the C435S mutant. Polypetide heterodimerization was confirmed by co-expression of Strep-tagged WT-ANGPT2 with Flag-tagged WT- or mutant ANGPT2 (Fig. 2F). Flag-tagged T299M and N304K mutants co-precipitated with the strep-tagged WT-ANGPT2 from the cell culture medium, whereas the C435S and R492Q mutants were only co-precipitated from the cell lysates. The N304K mutant was co-precipitated both from the cell culture medium and the cell lysates.

Oligomerization and TIE2 binding of ANGPT2 mutants

We next analyzed ANGPT2 oligomerization by western blotting of the supernatants of the transfected cells under non-reducing conditions. The T299M and N304K mutants formed covalent dimers and oligomers similar to WT-ANGPT2, in an approximately 2:1 ratio (fig. S2, B and C). Oligomerization of the C435S and R492Q mutants could not be analyzed because of their low secretion.

To test the effects of the mutations on ANGPT2 binding to TIE2, we produced WT and mutant ANGPT2 proteins in HEK293 cells and precipitated then from culture medium with ANGPT2 antibodies or a Fc-tagged TIE2 ligand-binding domain (Fig. 2, G and H). All ANGPT2 proteins, including small amounts of the C435S and R492Q mutants, were immunoprecipitated with the ANGPT2 antibody, whereas all except the C435S mutant were precipitated by TIE2-Fc. In TIE2 binding assays, the T299M and N304K mutants showed a similar affinity for TIE2 as the WT-ANGPT2 protein (fig. S2, D and E).

Angiopoietin oligomers consist of asymmetric homodimers

To test if the mutations found in patients with primary lymphedema affected ANGPT2 oligomerization and thereby TIE2 activation, we first undertook biophysical studies of WT-ANGPT1 and WT-ANGPT2 with and without the TIE2 ligand-binding domain. To obtain soluble, stable, and homogenous proteins that can form homodimers or homotrimers (*9, 41*), we created N-terminally truncated human ANGPT1[150-498] and ANGPT2[147-496] polypeptides containing the

majority of the predicted coiled-coil domains and the fibrinogen-like domains. These were analyzed by size exclusion chromatography with multi-angle laser light scattering (SEC-MALLS) alone and in complex with the TIE2 ligand-binding domain (Fig. 3, A and B). The data indicated that the ANGPT1$^{150-498}$ and ANGPT2$^{147-496}$ truncated proteins were dimers in solution (predicted molecular weight= 2x41 kDa), ANGPT1$^{150-498}$ without and ANGPT2$^{147-496}$ with some post-translational modifications. Both complexes with TIE2 ligand-binding domain displayed the 2:1 ANGPT-TIE2 stoichiometry.

To obtain structural models of the ANGPT dimers and their complexes with TIE2, we collected small angle X-ray scattering (SAXS) data from the purified proteins. We hypothesized that the homology between the angiopoietins and fibrinogen extended beyond the fibrinogen-like domain. Thus, we generated a structural model of ANGPT1$^{150-498}$ dimer for comparison (fig S3, A-D). An *ab initio* model derived from the SAXS data indicated that ANGPT1$^{150-498}$ is an extended molecule with two globular domains at the other end arranged in an asymmetrical fashion (Fig. 3, C and D). The expected scattering profile was consistent with the observed data, as indicated by the low chi-square value calculated by CRYSOL (*42*). We next generated a model for the ANGPT-TIE2 complex in 2:1 stoichiometry using the ANGPT1-TIE2 complex in PDB entry 4K0V (Fig. 3E). Again, the expected scattering profile calculated from the asymmetric ANGPT1$^{150-498}$-TIE2 complex model was in agreement with the observed data (Fig. 3F). Using the SREFLEX rigid-body refinement (*43*), we improved the fit of both the dimeric ANGPT1$^{150-498}$ and its TIE2 complex to the SAXS data by slightly adjusting the angle between the fibrinogen-like domain dimer and the coiled-coil domain (fig S4, A-G). Similarly, the SAXS data supported also the binding of the asymmetric ANGPT2$^{147-496}$ to TIE2 in a 2:1 stoichiometry (Fig. 3G).

The asymmetric dimerization of ANGPT polypeptides and their 2:1 stoichiometry with TIE2 suggest that dimers alone cannot activate TIE2. As expected, ANGPT1$^{150-498}$ and ANGPT2$^{147-496}$ induced essentially no TIE2 phosphorylation in human umbilical vein ECs (HUVECs) (fig. S5, A and B), and ANGPT2$^{147-496}$ decreased COMP-ANGPT1 (Cartilage oligomeric matrix protein fusion with the ANGPT1 fibrinogen-like domain (*44*))-induced phosphorylation of TIE2 when applied in a molar excess relative to COMP-ANGPT1 (fig. S5, C and D). Instead, the dimeric cartilage matrix protein (CMP)-ANGPT1 chimera is a potent TIE2 agonist (*45*). Consistent with

this, the SAXS analysis of CMP-ANGPT1 alone and in complex with the TIE2-LBD provided a model for CMP-ANGPT1-induced TIE2 dimerization in a 2:2 stoichiometry (fig. S6, A and B). These results indicate that the extended coiled-coil domains are responsible for the asymmetric ANGPT dimerization and 2:1 stoichiometry of TIE2 binding.

The T299M mutant is located in the ANGPT2 dimerization interface

The ANGPT2 dimerization model supported by the SAXS data indicated that Thr299 is located at the dimerization interface of the ANGPT2 fibrinogen-like domains and the larger sidechain of the Met299 mutant could induce steric clashes and affect dimerization (fig. S7, A and B). Comparison of the SAXS data obtained for the WT-ANGPT2 and T299M mutants under the same conditions indicated small but distinct differences in the distance distribution function and in the SAXS fitting score (χ^2), as defined in SASREF (fig. S7, C and D) (*46*) (*43*). This suggested that the T299M mutation induced subtle differences in ANGPT2 dimerization. The Thr299 residues in the ANGPT2 dimer are located between its integrin-α5 binding sites centered on Gln362 residues (*30*). This prompted us to investigate the effect of the T299M mutation on α5β1 integrin binding. Compared to WT-ANGPT2, the binding of the T299M mutant to the extracellular domain of intergrin-the α5 subunit was reduced in pull-down experiments (fig. S7, E and F).

We tested the effect of the T299M mutation on lymphatic vessels in vivo by transfecting the ears of 6-weeks-old mice with adeno-associated viral vectors (AAVs) encoding the WT or the T299M mutant ANGPT2. We analyzed the ears four weeks after the injection by whole-mount immunofluorescent staining for VEGFR-3. No obvious differences in the cutaneous lymphatic vessel network in the ear could be detected between the control vector and the WT-ANGPT2 injected mice (Fig. 4, A and B). In contrast, several areas of enlarged lymphatic vessels together with dense sprouting could be detected in the ears transfected with the T299M mutant ANGPT2. This resulted in significant increases in vessel area ($P = 0.005$), width ($P = 0.002$), skeleton length ($P = 0.03$), and a slight increase in the number of branching points ($P = 0.06$), indicating that the overexpression of the T299M mutant ANGPT2 promotes lymphangiogenesis in vivo.

Function of patient mutant ANGPT2s in autocrine and paracrine TIE2 activation

11

Although ANGPT2 was initially described as a TIE2 antagonist, it was later characterized as a weak autocrine agonist of TIE2 under certain conditions (*13, 14, 47, 48*). We tested the capability of TIE2 activation by WT-ANGPT2 and the T299M and N304K mutants by stimulating HUVECs with purified recombinant proteins. Unlike COMP-ANGPT1, WT-ANGPT2 and the T299M and N304K ANGPT2 mutants did not induce paracrine TIE2 phosphorylation (fig. S8A). Notably, recombinant ANGPT2 induced a weak activation of TIE2 in LECs (fig. S8B), in line with previous publications (*18-20, 27, 49*).

To mimic the autocrine signaling of EC ANGPT2, we expressed ANGPT2 mutants in HUVECs, LECs, and HUVECs expressing lentivirally-transfected TIE2 (Fig. 5A and B, fig. S9, A-C, fig. S10 A-C). Immunofluorescent staining showed that, as in HEK293 cells, the C435S and R492Q ANGPT2 mutants resulted in intracellular aggregates also in ECs (Fig. 5A, fig. S9A). However, WT-ANGPT2 and the T299M and N304K mutants showed diffuse fluorescence on the cell surface and co-localized with TIE2 at cell-cell junctions, as described previously for WT-ANGPT2 (*15, 27*). Despite prominent co-localization with TIE2 in the double-transfected cells, WT or the mutant ANGPT2 did not induce increased TIE2 phosphorylation (fig. S9B). In the autocrine expression assay, phosphorylation of the endogenous TIE2 was observed in HUVECs and in LECs transfected with WT-ANGPT2 (P = 0.022 in LECs) and with the T299M, N304K, and R492Q mutants (fig. S9C, Fig. 5B). Autocrine WT-ANGPT2 and the T299M (*P* < 0.05) mutant promoted also TIE1 activation in LECs (Fig. 5C).

Discussion

Primary lymphedema can be caused by inactivating mutations in the VEGFR3 *(FLT4)* gene or LOF mutations in proteins affecting VEGFR3 signaling (*1-3, 6*). Here we report mutations in the second endothelial growth factor receptor pathway through the identification of ANGPT2 mutations in individuals affected by primary lymphedema. Both Angpt1 and Angpt2 ligands, as well as their receptors Tie1 and Tie2, are known to promote lymphangiogenesis in mice (*18-21, 24-27, 50, 51*). The mutations that we identified in patients with primary lymphedema affected ANGPT2 function variably; one mutation was a LOF (haploinsufficiency) allele, three out of the four amino acid substitutions resulted in LOF with a dominant negative effect, and the remaining amino acid

substitution reduced ANGPT2 binding to integrins (table S1). Our analyses also provided a structural explanation for the need of angiopoietin oligomers in TIE2 activation, and an autocrine model for ANGPT2-mediated TIE2 and TIE1 activation in LECs.

The five heterozygous mutations in *ANGPT2* identified in our cohort of 543 patients from distinct families represent 0.9% of the primary lymphedema cases. Two of the substitutions are absent in large genetic databases (gnomAD), containing almost 200,000 whole exome- or genome-sequenced individuals) and the other two are very rare (0.02% of the alleles at these positions). We performed whole-exome sequencing for patients LE-623-10, LE-128-10, and LE-148-1000, but detected no other putative lymphedema-causing mutations in them. Each ANGPT2 substitution affected a conserved amino acid position that was predicted to be deleterious for ANGPT2 function by four to six different algorithms, on the basis of sequence conservation, charge, nature of the original and modified amino acid residues, the affected functional domains, and structural position within the protein. Moreover, this conclusion is supported by the fact that the *ANGPT2* gene has a high predicted LOF-intolerance score.

Clinically, lymphedema in the seven affected patients of these five families had characteristics similar to Nonne-Milroy disease caused by mutant VEGFR3, in which lymphedema is autosomal dominant with reduced penetrance, congenital and tends to resorb with time. Penetrance was indeed reduced in two of the five ANGPT2-mutated families, onset occurred at birth or less than one year of age in six of the seven ANGPT2 patients, and the lymphedema tended to resorb in all ANGPT2-mutated families, except family LE-128 with the T299M mutation, in which lymphedema progressed and was associated with episodes of cellulitis. Hydrocele was also present in four of the five male patients.

Based on the limited number of cases examined here, it is difficult to make genotype-phenotype correlations. In family LE-148, lymphedema was not limited to lower extremities, but also present in hands. The C435S mutation found in this family appeared to be the most penetrant of the identified mutations and was the most strongly sequestered mutant protein inside the cells. It also had a dominant-negative effect on WT-ANGPT2 secretion. The phenotype associated with the R492Q mutation (LE-623) appeared somewhat weaker, as one mutation carrier was unaffected,

and the index patient had limited congenital lymphedema that largely resorbed with time. The other clinical features of patient LE-623 (intellectual disability and facial dysmorphism) could be due to additional genetic defects yet to be identified, although molecular karyotyping did not reveal any chromosomal anomalies. The N304K mutation was associated with bilateral congenital primary lymphedema, mimicking classic Nonne-Milroy disease. The T299M mutant protein was secreted normally from transfected ECs, but induced abnormal lymphatic vessel changes in vivo and was the only ANGPT2 mutant associating with progressive lymphedema, suggesting that it causes deterioration of lymphatic function over time, perhaps by inducing hyperplasia.

The ANGPT2 substitution mutations were all in the TIE2-binding fibrinogen-like domain. Structural analysis implied that C435S and R492Q led to severe changes in protein folding and identified Asn304 as a potential N-glycosylation site. These three mutants showed reduced secretion from HEK293 and LEC cells, and C435S also failed to bind TIE2. The mutations did not affect the covalent dimer/oligomer ratio. The reduced secretion and apparent polypeptide size difference of N304K reflects indeed an altered glycosylation pattern, which may be functionally important, similar to the N-glycosylation in the dimeric CMP-ANGPT1 (*45*). The secretion-deficient mutants reduced overall ANGPT2 secretion, which may cause a dominant-negative effect. Patient LE-623-10 with a R492Q mutation had a 40% reduction in plasma ANGPT2 .

To better understand the effect of the mutations on ANGPT2 oligomerization, we undertook biophysical studies of N-terminally truncated ANGPTs, alone and in complex with TIE2-LBD. The N-terminally truncated ANGPT1$^{150-498}$ and ANGPT2$^{147-496}$ proteins lack the super clustering domains, which are responsible for the heterogeneity of the higher-order oligomers (*9, 41*). SAXS data indicated that both the truncated ANGPT1 and ANGPT2 formed highly elongated asymmetric dimers that bind TIE2 in a 2:1 stoichiometry, and both behaved as TIE2 antagonists in cultured human primary ECs. These data strongly suggest also that naturally occurring ANGPT dimers are antagonists of TIE2 in *cis* and in *trans* activation (*52, 53*). In comparison to ANGPT1, a much smaller fraction of ANGPT2 occurs as high-order oligomers connected by their N-terminal SCDs (*41*), suggesting that the higher fraction of ANGPT2 dimers may account for its lower TIE2 activity.

Our present SAXS results in combination with the previously published crystal structures and TIE2 clustering scheme (*54, 55*) allow validation of the N-terminally truncated ANGPT-TIE interactions. On the basis of the SAXS data, the superimposed ANGPT dimers bound to opposite sides of the clustered TIE dimers are oriented so that the N-termini almost meet each other. The two dimers, if connected by the super clustering domains, would create a tetrameric ANGPT1 that is similar to that visualized by EM (*9*). However, the connected ANGPT dimers would not bind to the same TIE2 dimer. Instead, they would be intervened by one or more TIE2 dimers. This may reflect the flexibility in TIE2 (*54, 55*), but it is also possible that TIE1 could instead be embedded as an intervening receptor. It is also notable that the integrin-α5 binding sites in the ANGPT2 dimers in this TIE2 clustering model are accessible for simultaneous integrin binding. This therefore creates a model to further investigate the interplay between TIE1, TIE2, integrin-α5, and the ANGPTs.

ANGPT2 is secreted by ECs as an autocrine TIE2 ligand. To test the effect of our ANGPT2 mutants on TIE2 activation, we established a model for autocrine activation of TIE2. Co-transfection with TIE2 revealed that the T299M and N304K mutants, like WT-ANGPT2, show prominent junctional co-localization with TIE2. The WT and soluble ANGPT2 mutants induced autocrine TIE2 activation when transfected to either HUVECs or LECs. ANGPT2 also induced TIE1 activation in LECs, suggesting that ANGPT2 is indeed a TIE1 and TIE2 agonist in LECs, which, unlike blood vascular endothelial cells (BECs), lack VE-PTP (*27*). This means that Angpt2-stimulated activation of TIE1, which is expressed in the lymphatic vasculature throughout embryonic development, could be crucial for lymphatic remodeling and maturation (*21, 24-26*). Thus, mutations in ANGPT2 are likely to affect both TIE2 and TIE1 activation in lymphatic vessels, and the ANGPT2 haploinsufficiency represents a LOF mutation. The N304K, C435S, and R492Q mutants of ANGPT2 also inhibited the secretion of the WT allele in vitro, which may have a dominant-negative effect on ANGPT2 signaling in the heterozygous state. Therefore, also these three mutations are LOF. ANGPT2 LOF mutations in humans may act similarly to the ANGPT2-blocking antibodies previously tested in mouse embryos, by affecting the formation of button-type LEC junctions, adherens junction stability, or lymphatic valve formation and maturation during collecting lymphatic vessel development (*20*).

Some limitations exist to our study. First, the effects of the T299M mutant on the ANGPT2-integrin-α5 signaling pathway remain to be fully understood. This mutant had no obvious secretion deficiency and activated TIE2 and TIE1 in LECs as well as WT-ANGPT2. Our in vivo assay suggested that the T299M mutant is hypermorphic, as the expression of AAV encoding the T299M mutant induced a more hyperplastic lymphatic vessel network in mouse skin than expression of WT-ANGPT2. Our analysis of ANGPT2-integrin-α5 binding by the T299M mutant is consistent with the report that deletion of the *Itga5* gene during lymphatic vascular development leads to lymphatic vessel dilation and tissue edema in mice (*56*). Furthermore, although the R492Q mutant ANGPT2 decreased secretion and also inhibited the secretion of WT-ANGPT2, it induced TIE2 activation in ECs, likely due to its enhanced secretion via heterodimerization with endogenous ANGPT2. The C435S mutant could also be detected in LEC supernatant, but unlike the R492Q mutant, it did not bind to or activate TIE2. We found that patient LE-623-10 with a R492Q mutation had a 40% reduction in plasma ANGPT2 compared to three healthy controls. Future studies should show if ANGPT2 concentrations in plasma prove useful in the diagnosis of the mutant alleles.

In summary, we identified *ANGPT2* mutations with a dominant pattern of inheritance and variable penetrance in patients with primary lymphedema. Our functional and genetic characterization of these mutants clarify the role of ANGPT2 in TIE2 and TIE1 signaling. Because ANGPT2 functions as an autocrine TIE2 and TIE1 agonist lymphatic endothelium, our results indicate that ANGPT2 haploinsufficiency, LOF mutations, or hypermorphic alleles may contribute to primary lymphedema with incomplete penetrance in humans. Moreover, our structural data on asymmetric ANGPT homodimers that bind only one TIE2 receptor polypeptide indicate that oligomerization via the super clustering domain is a prerequisite for TIE2 dimerization and activation by both ANGPT1 and ANGPT2. Our structural data also suggests that naturally occurring ANGPT dimers are likely TIE2 antagonists.

Materials and Methods

Study design

The goal of this study was to investigate whether mutations in ANGPT2 could contribute to the onset of primary lymphedema. We identified mutations in the *ANGPT2* gene in a cohort of 543

index patients with primary lymphedema. We explored the mechanistic role of the ANGPT2 mutations in the TIE2 and TIE1 signaling pathway in vitro by analyzing the expression and secretion and TIE2 and TIE1 activation in LECs. We further explored the structural basis of ANGPT oligomerization and TIE2 complex formation to better understand the effects of the ANGPT2 mutations in oligomeric ANGPT2. We also analyzed the effect of T299M in vivo using AAV-mediated gene transfer in mice. The National Animal Experiment Board in Finland approved all experiments involving mice. Mice were housed in individually ventilated cages with enrichment materials in a facility following the guidelines by the Federation of European Laboratory Animal Science Associations. AAV injection experiments and biomarker analysis were conducted in a fully blinded fashion. Informed consent was obtained from all participants and the studies were approved by the ethical committee of UCLouvain, Brussels, Belgium, and the review boards of the clinical collaborators.

Statistical analysis

Data are expressed as mean ± SEM and statistical evaluation was performed using Mann-Whitney test or one-way ANOVA, followed by Kruskal-Wallis *post hoc* pairwise test where appropriate, using GraphPad Prism version 6.00 for Mac OSX (GraphPad Software). All data from the western blots were normalized before quantification using either a standard COMP-ANGPT1 treatment or a standard ANGPT2 protein sample. $P < 0.05$ was considered statistically significant.

Supplementary Materials:

Materials and Methods

Fig. S1. Structural characterization of ANGPT2 mutations.

Fig. S2. Characterization of the oligomerization and TIE2 binding of ANGPT2 mutants.

Fig. S3. A fibrinogen-based homology model of dimeric ANGPT1[150-498].

Fig. S4. SAXS analysis of the N-terminally truncated ANGPT1[150-498] and ANGPT2[147-496].

Fig. S5. Dimeric angiopoietins are TIE2 antagonists.

Fig. S6. SAXS analysis of the dimeric CMP-ANGPT1 and its complex with TIE2 ligand-binding domain.

Fig. S7. The T299M mutation is located in the dimerization interface of ANGPT2 fibrinogen-like domains and shows decreased integrin-α5 binding.

Fig. S8. Paracrine ANGPT2 is a TIE2 antagonist in HUVECs but a weak agonist in LECs.

Fig. S9. ANGPT2 mutations led to reduced expression or secretion and aberrant trafficking of ANGPT2.

Fig. S10. ANGPT1 tetramer and TIE2 clustering.

Table S1. Summary of the functional impact of the mutations found in patients with primary lymphedema.

Data file S1. Primary data.

References and notes:

1. M. J. Karkkainen, R. E. Ferrell, E. C. Lawrence, M. A. Kimak, K. L. Levinson, M. A. McTigue, K. Alitalo, D. N. Finegold, Missense mutations interfere with VEGFR-3 signalling in primary lymphoedema. *Nat. Genet.* **25**, 153-159 (2000).
2. A. Irrthum, M. J. Karkkainen, K. Devriendt, K. Alitalo, M. Vikkula, Congenital hereditary lymphedema caused by a mutation that inactivates VEGFR3 tyrosine kinase. *Am. J. Hum. Genet.* **67**, 295-301 (2000).
3. K. Alitalo, T. Tammela, T. V. Petrova, Lymphangiogenesis in development and human disease. *Nature* **438**, 946-953 (2005).
4. J. Kazenwadel, K. L. Betterman, C. E. Chong, P. H. Stokes, Y. K. Lee, G. A. Seeker, Y. Agalarov, C. S. Demir, D. M. Lawrence, D. L. Sutton, S. P. Tabruyn, N. Miura, M. Salminen, T. V. Petrova, J. M. Matthews, C. N. Hahn, H. S. Scott, N. L. Harvey, GATA2 is required for lymphatic vessel valve development and maintenance. *J. Clin. Invest.* **125**, 2979-2994 (2015).
5. P. Brouillard, L. Boon, M. Vikkula, Genetics of lymphatic anomalies. *J. Clin. Invest.* **124**, 898-904 (2014).
6. P. Brouillard, L. Dupont, R. Helaers, R. Coulie, G. E. Tiller, J. Peeden, A. Colige, M. Vikkula, Loss of ADAMTS3 activity causes Hennekam lymphangiectasia-lymphedema syndrome 3. *Hum. Mol. Genet.* **26**, 4095-4104 (2017).
7. H. G. Augustin, G. Y. Koh, G. Thurston, K. Alitalo, Control of vascular morphogenesis and homeostasis through the angiopoietin-Tie system. *Nat. Rev. Mol. Cell. Biol.* **10**, 165-177 (2009).
8. P. Saharinen, M. Jeltsch, M. M. Santoyo, V. M. Leppänen, K. Alitalo, in *Receptor Tyrosine Kinases: Family and Subfamilies*. (2015), vol. 861, pp. 743-775.
9. S. Davis, N. Papadopoulos, T. H. Aldrich, P. C. Maisonpierre, T. Huang, L. Kovac, A. Xu, R. Leidich, E. Radziejewska, A. Rafique, J. Goldberg, V. Jain, K. Bailey, M. Karow, J. Fandl, S. J. Samuelsson, E. Ioffe, J. S. Rudge, T. J. Daly, C. Radziejewski, G. D. Yancopoulos, Angiopoietins have distinct modular domains essential for receptor binding, dimerization and superclustering. *Nat. Struct. Biol.* **10**, 38-44 (2003).
10. C. Suri, P. F. Jones, S. Patan, S. Bartunkova, P. C. Maisonpierre, S. Davis, T. N. Sato, G. D. Yancopoulos, Requisite role of angiopoietin-1, a ligand for the TIE2 receptor, during embryonic angiogenesis. *Cell* **87**, 1171-1180 (1996).
11. S. Davis, T. H. Aldrich, P. F. Jones, A. Acheson, D. L. Compton, V. Jain, T. E. Ryan, J. Bruno, C. Raziejewski, P. C. Maisonpierre, G. D. Yancopoulos, Isolation of Angiopoietin-

1, a Ligand for the TIE2 receptor, by Secretion-Trap Expression Cloning. *Cell* **87**, 1161-1169 (1996).

12. U. Fiedler, M. Scharpfenecker, S. Koidl, A. Hegen, V. Grunow, J. M. Schmidt, W. Kriz, G. Thurston, H. G. Augustin, The Tie-2 ligand angiopoietin-2 is stored in and rapidly released upon stimulation from endothelial cell Weibel-Palade bodies. *Blood* **103**, 4150-4156 (2004).

13. M. Scharpfenecker, U. Fiedler, Y. Reiss, H. G. Augustin, The Tie-2 ligand angiopoietin-2 destabilizes quiescent endothelium through an internal autocrine loop mechanism. *J. Cell Sci.* **118**, 771-780 (2005).

14. P. C. Maisonpierre, C. Suri, P. F. Jones, S. Bartunkova, S. J. Wiegand, C. Radziejewski, D. Compton, J. McClain, T. H. Aldrich, N. Papadopoulos, T. J. Daly, S. Davis, T. N. Sato, G. D. Yancopoulos, Angiopoietin-2, a natural antagonist for Tie2 that disrupts in vivo angiogenesis. *Science* **277**, 55-60 (1997).

15. E. A. Korhonen, A. Lampinen, H. Giri, A. Anisimov, M. Kim, B. Allen, S. Fang, G. D'Amico, T. J. Sipila, M. Lohela, T. Strandin, A. Vaheri, S. Yla-Herttuala, G. Y. Koh, D. M. McDonald, K. Alitalo, P. Saharinen, Tie1 controls angiopoietin function in vascular remodeling and inflammation. *J. Clin. Invest.* **126**, 3495-3510 (2016).

16. J. Holash, P. C. Maisonpierre, D. Compton, P. Boland, C. R. Alexander, D. Zagzag, G. D. Yancopoulos, S. J. Wiegand, Vessel cooption, regression, and growth in tumors mediated by angiopoietins and VEGF. *Science* **284**, 1994-1998 (1999).

17. P. Saharinen, L. Eklund, K. Alitalo, Therapeutic targeting of the angiopoietin-TIE pathway. *Nat. rev. Drug disc.* **16**, 635-661 (2017).

18. N. W. Gale, G. Thurston, S. F. Hackett, R. Renard, Q. Wang, J. McClain, C. Martin, C. Witte, M. H. Witte, D. Jackson, C. Suri, P. A. Campochiaro, S. J. Wiegand, G. D. Yancopoulos, Angiopoietin-2 is required for postnatal angiogenesis and lymphatic patterning, and only the latter role is rescued by Angiopoietin-1. *Dev. Cell* **3**, 411-423 (2002).

19. M. Dellinger, R. Hunter, M. Bernas, N. Gale, G. Yancopoulos, R. Erickson, M. Witte, Defective remodeling and maturation of the lymphatic vasculature in Angiopoietin-2 deficient mice. *Dev. Biol.* **319**, 309-320 (2008).

20. W. Zheng, H. Nurmi, S. Appak, A. Sabine, E. Bovay, E. A. Korhonen, F. Orsenigo, M. Lohela, G. D'Amico, T. Holopainen, C. C. Leow, E. Dejana, T. V. Petrova, H. G. Augustin, K. Alitalo, Angiopoietin 2 regulates the transformation and integrity of lymphatic endothelial cell junctions. *Genes Dev.* **28**, 1592-1603 (2014).

21. B. Shen, Z. Shang, B. Wang, L. Zhang, F. Zhou, T. Li, M. Chu, H. Jiang, Y. Wang, T. Qiao, J. Zhang, W. Sun, X. Kong, Y. He, Genetic dissection of tie pathway in mouse lymphatic maturation and valve development. *Arterioscler. Thromb. Vasc. Biol.* **34**, 1221-1230 (2014).

22. D. Yuen, S. Grimaldo, R. Sessa, T. Ecoiffier, T. Truong, E. Huang, M. Bernas, S. Daley, M. Witte, L. Chen, Role of angiopoietin-2 in corneal lymphangiogenesis. *Invest. Ophthalmol. Vis. Sci.* **55**, 3320-3327 (2014).

23. G. D'Amico, E. A. Korhonen, A. Anisimov, G. Zarkada, T. Holopainen, R. Hagerling, F. Kiefer, L. Eklund, R. Sormunen, H. Elamaa, R. A. Brekken, R. H. Adams, G. Y. Koh, P. Saharinen, K. Alitalo, Tie1 deletion inhibits tumor growth and improves angiopoietin antagonist therapy. *J. Clin. Invest.* **124**, 824-834 (2014).

24. X. Qu, K. Tompkins, L. E. Batts, M. Puri, H. S. Baldwin, Abnormal embryonic lymphatic vessel development in Tie1 hypomorphic mice. *Development* **137**, 1285-1295 (2010).

25.	G. D'Amico, E. A. Korhonen, M. Waltari, P. Saharinen, P. Laakkonen, K. Alitalo, Loss of endothelial Tie1 receptor impairs lymphatic vessel development-brief report. *Arterioscler. Thromb. Vasc. Biol.* **30**, 207-209 (2010).

26.	X. H. Qu, B. Zhou, H. S. Baldwin, Tie1 is required for lymphatic valve and collecting vessel development. *Dev. Biol.* **399**, 117-128 (2015).

27.	T. Souma, B. R. Thomson, S. Heinen, I. Anna Carota, S. Yamaguchi, T. Onay, P. Liu, A. K. Ghosh, C. Li, V. Eremina, Y. K. Hong, A. N. Economides, D. Vestweber, K. G. Peters, J. Jin, S. E. Quaggin, Context-dependent functions of angiopoietin 2 are determined by the endothelial phosphatase VEPTP. *Proc. Natl. Acad. Sci. USA* **115**, 1298-1303 (2018).

28.	M. Winderlich, L. Keller, G. Cagna, A. Broermann, O. Kamenyeva, F. Kiefer, U. Deutsch, A. F. Nottebaum, D. Vestweber, VE-PTP controls blood vessel development by balancing Tie-2 activity. *J. Cell. Biol.* **185**, 657-671 (2009).

29.	M. Felcht, R. Luck, A. Schering, P. Seidel, K. Srivastava, J. H. Hu, A. Bartol, Y. Kienast, C. Vettel, E. K. Loos, S. Kutschera, S. Bartels, S. Appak, E. Besemfelder, D. Terhardt, E. Chavakis, T. Wieland, C. Klein, M. Thomas, A. Uemura, S. Goerdt, H. G. Augustin, Angiopoietin-2 differentially regulates angiogenesis through TIE2 and integrin signaling. *J. Clin. Invest.* **122**, 1991-2005 (2012).

30.	H. S. Lee, S. J. Oh, K. H. Lee, Y. S. Lee, E. Ko, K. E. Kim, H. C. Kim, S. Kim, P. H. Song, Y. I. Kim, C. Kim, S. Han, Gln-362 of Angiopoietin-2 Mediates Migration of Tumor and Endothelial Cells through Association with alpha 5 beta 1 Integrin. *J. Biol. Chem.* **289**, 31330-31340 (2014).

31.	L. Hakanpaa, T. Sipila, V. M. Leppanen, P. Gautam, H. Nurmi, G. Jacquemet, L. Eklund, J. Ivaska, K. Alitalo, P. Saharinen, Endothelial destabilization by angiopoietin-2 via integrin beta1 activation. *Nat. Commun.* **6**, 5962 (2015).

32.	A. C. Mirando, J. Shen, E. S. R. Lima, Z. Chu, N. Sass, V. E. Lorenc, J. J. Green, P. A. Campochiaro, A. S. Popel, N. B. Pandey, A collagen IV-derived peptide disrupts alpha5beta1 integrin and potentiates Ang2-Tie2 signaling. *JCI Insight* **4**, (2019).

33.	M. Vikkula, L. M. Boon, K. L. Carraway, 3rd, J. T. Calvert, A. J. Diamonti, B. Goumnerov, K. A. Pasyk, D. A. Marchuk, M. L. Warman, L. C. Cantley, J. B. Mulliken, B. R. Olsen, Vascular dysmorphogenesis caused by an activating mutation in the receptor tyrosine kinase TIE2. *Cell* **87**, 1181-1190 (1996).

34.	T. Souma, S. W. Tompson, B. R. Thomson, O. M. Siggs, K. Kizhatil, S. Yamaguchi, L. Feng, V. Limviphuvadh, K. N. Whisenhunt, S. Maurer-Stroh, T. L. Yanovitch, L. Kalaydjieva, D. N. Azmanov, S. Finzi, L. Mauri, S. Javadiyan, E. Souzeau, T. Zhou, A. W. Hewitt, B. Kloss, K. P. Burdon, D. A. Mackey, K. F. Allen, J. B. Ruddle, S. H. Lim, S. Rozen, K. N. Tran-Viet, X. Liu, S. John, J. L. Wiggs, F. Pasutto, J. E. Craig, J. Jin, S. E. Quaggin, T. L. Young, Angiopoietin receptor TEK mutations underlie primary congenital glaucoma with variable expressivity. *J. Clin. Invest.* **126**, 2575-2587 (2016).

35.	N. Limaye, V. Wouters, M. Uebelhoer, M. Tuominen, R. Wirkkala, J. B. Mulliken, L. Eklund, L. M. Boon, M. Vikkula, Somatic mutations in angiopoietin receptor gene TEK cause solitary and multiple sporadic venous malformations. *Nat. Genet.* **41**, 118-124 (2009).

36.	J. Soblet, J. Kangas, M. Natynki, A. Mendola, R. Helaers, M. Uebelhoer, M. Kaakinen, M. Cordisco, A. Dompmartin, O. Enjolras, S. Holden, A. D. Irvine, L. Kangesu, C. Leaute-Labreze, A. Lanoel, Z. Lokmic, S. Maas, M. A. McAleer, A. Penington, P. Rieu, S. Syed, C. van der Vleuten, R. Watson, S. J. Fishman, J. B. Mulliken, L. Eklund, N. Limaye, L. M.

Boon, M. Vikkula, Blue Rubber Bleb Nevus (BRBN) Syndrome Is Caused by Somatic TEK (TIE2) Mutations. *J. Invest. Dermatol.* **137**, 207-216 (2017).

37. V. Bafunno, D. Firinu, M. D'Apolito, G. Cordisco, S. Loffredo, A. Leccese, M. Bova, M. P. Barca, R. Santacroce, M. Cicardi, S. Del Giacco, M. Margaglione, Mutation of the angiopoietin-1 gene (ANGPT1) associates with a new type of hereditary angioedema. *J. Allergy Clin. Immunol.* **141**, 1009-1017 (2018).

38. B. R. Thomson, T. Souma, S. W. Tompson, T. Onay, K. Kizhatil, O. M. Siggs, L. Feng, K. N. Whisenhunt, T. L. Yanovitch, L. Kalaydjieva, D. N. Azmanov, S. Finzi, C. E. Tanna, A. W. Hewitt, D. A. Mackey, Y. S. Bradfield, E. Souzeau, S. Javadiyan, J. L. Wiggs, F. Pasutto, X. Liu, S. W. John, J. E. Craig, J. Jin, T. L. Young, S. E. Quaggin, Angiopoietin-1 is required for Schlemm's canal development in mice and humans. *J. Clin. Invest.* **127**, 4421-4436 (2017).

39. N. J. Meyer, M. Li, R. Feng, J. Bradfield, R. Gallop, S. Bellamy, B. D. Fuchs, P. N. Lanken, S. M. Albelda, M. Rushefski, R. Aplenc, H. Abramova, E. N. Atochina-Vasserman, M. F. Beers, C. S. Calfee, M. J. Cohen, J. F. Pittet, D. C. Christiani, G. E. O'Keefe, L. B. Ware, A. K. May, M. M. Wurfel, H. Hakonarson, J. D. Christie, ANGPT2 Genetic Variant Is Associated with Trauma-associated Acute Lung Injury and Altered Plasma Angiopoietin-2 Isoform Ratio. *Am. J. Resp. Crit. Care Med.* **183**, 1344-1353 (2011).

40. E. Fastre, L. E. Lanteigne, R. Helaers, G. Giacalone, N. Revencu, D. Dionyssiou, E. Demiri, P. Brouillard, M. Vikkula, Splice-site mutations in VEGFC cause loss of function and Nonne-Milroy-like primary lymphedema. *Clin. Genet.* **94**, 179-181 (2018).

41. K. T. Kim, H. H. Choi, M. O. Steinmetz, B. Maco, R. A. Kammerer, S. Y. Ahn, H. Z. Kim, G. M. Lee, G. Y. Koh, Oligomerization and multimerization are critical for angiopoietin-1 to bind and phosphorylate Tie2. *J. Biol. Chem.* **280**, 20126-20131 (2005).

42. D. Svergun, C. Barberato, M. H. J. Koch, CRYSOL - A program to evaluate x-ray solution scattering of biological macromolecules from atomic coordinates. *J Appl Crystallogr* **28**, 768-773 (1995).

43. M. V. Petoukhov, D. I. Svergun, Analysis of X-ray and neutron scattering from biomacromolecular solutions. *Curr. Op. Struct. Biol.* **17**, 562-571 (2007).

44. C. H. Cho, R. A. Kammerer, H. J. Lee, M. O. Steinmetz, Y. S. Ryu, S. H. Lee, K. Yasunaga, K. T. Kim, I. Kim, H. H. Choi, W. Kim, S. H. Kim, S. K. Park, G. M. Lee, G. Y. Koh, COMP-Ang1: a designed angiopoietin-1 variant with nonleaky angiogenic activity. *Proc. Natl. Acad. Sci. USA* **101**, 5547-5552 (2004).

45. N. Oh, K. Kim, S. J. Kim, I. Park, J. E. Lee, Y. S. Seo, H. J. An, H. M. Kim, G. Y. Koh, A Designed Angiopoietin-1 Variant, Dimeric CMP-Ang1 Activates Tie2 and Stimulates Angiogenesis and Vascular Stabilization in N-glycan Dependent Manner. *Sci. Rep.* **5**, 15291 (2015).

46. M. V. Petoukhov, D. I. Svergun, Global rigid body modeling of macromolecular complexes against small-angle scattering data. *Biophys J* **89**, 1237-1250 (2005).

47. C. Daly, E. Pasnikowski, E. Burova, V. Wong, T. H. Aldrich, J. Griffiths, E. Ioffe, T. J. Daly, J. P. Fandl, N. Papadopoulos, D. M. McDonald, G. Thurston, G. D. Yancopoulos, J. S. Rudge, Angiopoietin-2 functions as an autocrine protective factor in stressed endothelial cells. *Proc. Natl. Acad. Sci. USA* **103**, 15491-15496 (2006).

48. H. T. Yuan, E. V. Khankin, S. A. Karumanchi, S. M. Parikh, Angiopoietin 2 is a partial agonist/antagonist of Tie2 signaling in the endothelium. *Mol. Cell. Biol* **29**, 2011-2022 (2009).

49. S. H. Song, K. L. Kim, K. A. Lee, W. Suh, Tie1 regulates the Tie2 agonistic role of angiopoietin-2 in human lymphatic endothelial cells. *Biochem. Biophys. Res. Comm.* **419**, 281-286 (2012).

50. T. Tammela, A. Saaristo, M. Lohela, T. Morisada, J. Tornberg, C. Norrmen, Y. Oike, K. Pajusola, G. Thurston, T. Suda, S. Yla-Herttuala, K. Alitalo, Angiopoietin-1 promotes lymphatic sprouting and hyperplasia. *Blood* **105**, 4642-4648 (2005).

51. T. Holopainen, P. Saharinen, G. D'Amico, A. Lampinen, L. Eklund, R. Sormunen, A. Anisimov, G. Zarkada, M. Lohela, H. Helotera, T. Tammela, L. E. Benjamin, S. Yla-Herttuala, C. C. Leow, G. Y. Koh, K. Alitalo, Effects of angiopoietin-2-blocking antibody on endothelial cell-cell junctions and lung metastasis. *J. Natl. Cancer Inst.* **104**, 461-475 (2012).

52. P. Saharinen, L. Eklund, J. Miettinen, R. Wirkkala, A. Anisimov, M. Winderlich, A. Nottebaum, D. Vestweber, U. Deutsch, G. Y. Koh, B. R. Olsen, K. Alitalo, Angiopoietins assemble distinct Tie2 signalling complexes in endothelial cell-cell and cell-matrix contacts. *Nat. Cell. Biol.* **10**, 527-537 (2008).

53. S. Fukuhara, K. Sako, T. Minami, K. Noda, H. Z. Kim, T. Kodama, M. Shibuya, N. Takakura, G. Y. Koh, N. Mochizuki, Differential function of Tie2 at cell-cell contacts and cell-substratum contacts regulated by angiopoietin-1. *Nat. Cell Biol.* **10**, 513-526 (2008).

54. V. M. Leppanen, P. Saharinen, K. Alitalo, Structural basis of Tie2 activation and Tie2/Tie1 heterodimerization. *Proc. Natl. Acad. Sci. USA* **114**, 4376-4381 (2017).

55. J. O. Moore, M. A. Lemmon, K. M. Ferguson, Dimerization of Tie2 mediated by its membrane-proximal FNIII domains. *Proc. Natl. Acad. Sci. USA* **114**, 4382-4387 (2017).

56. C. J. Turner, K. Badu-Nkansah, D. Crowley, A. van der Flier, R. O. Hynes, Integrin-alpha5beta1 is not required for mural cell functions during development of blood vessels but is required for lymphatic-blood vessel separation and lymphovenous valve formation. *Dev. Biol.* **392**, 381-392 (2014).

57. J. A. Montoya-Zegarra, E. Russo, P. Runge, M. Jadhav, A. H. Willrodt, S. Stoma, S. F. Norrelykke, M. Detmar, C. Halin, AutoTube: a novel software for the automated morphometric analysis of vascular networks in tissues. *Angiogenesis* **22**, 223-236 (2019).

Data and materials availability: All data associated with this study are present in the paper or the Supplementary Materials.

Figure legends
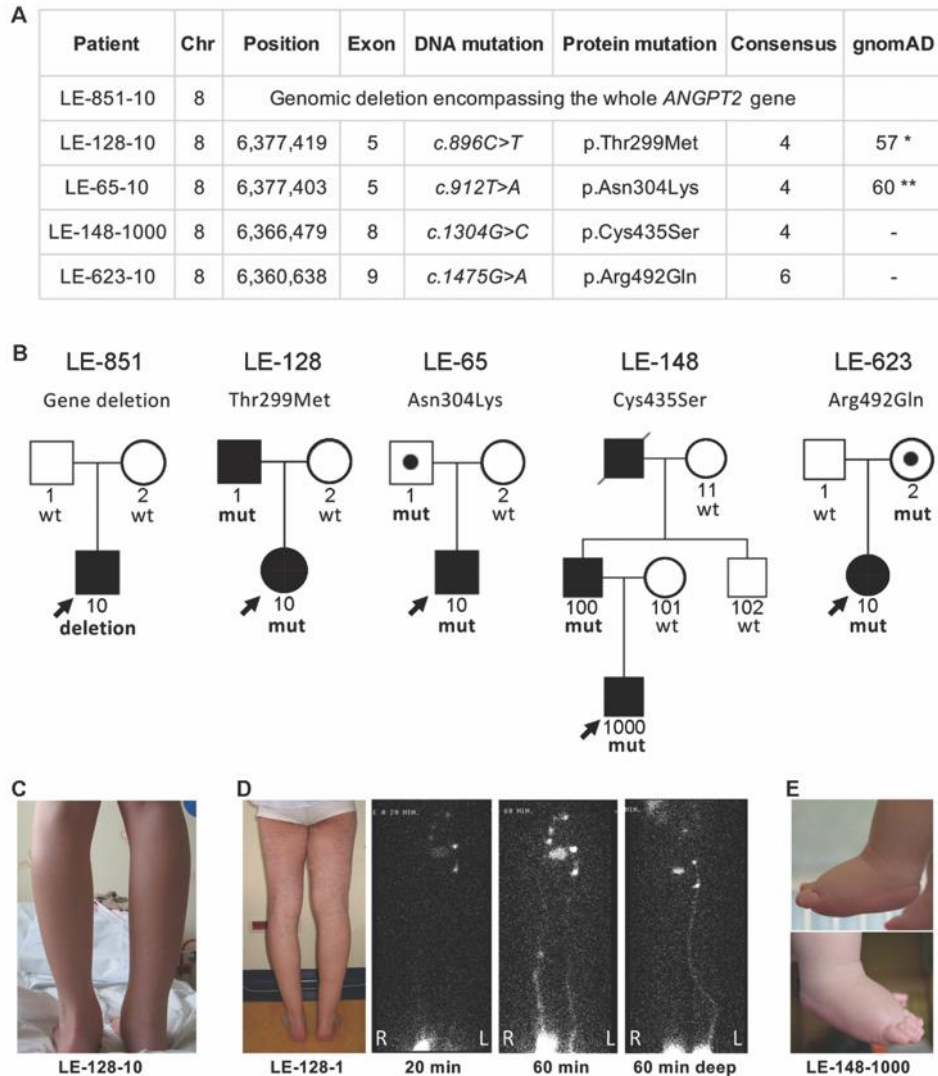
Fig. 1. ANGPT2 mutations in patients with primary lymphedema. (**A**) Whole-gene deletion and four variants found in five index cases. Consensus: number of software tools predicting the change as damaging, out of eight. The gnomAD repository collects variants of healthy individuals (* out of 251,418 and ** 282,800 alleles, 0.02% each). (**B**) Pedigrees of the five families showing co-segregation of the mutations. Arrows, index cases. Affected individuals are shown in black. Patients LE-65-1 and LE-623-2 were unaffected carriers of the mutations. (**C**) Right leg lymphedema in LE-128-10. (**D**) Right leg lymphedema in LE-128-1 and lymphoscintigraphy illustrating surface lymphatics (20 and 60 min post-injection) and deeper lymphatics (60 min). (**E**) Lower limb lymphedema in LE-148-1000.
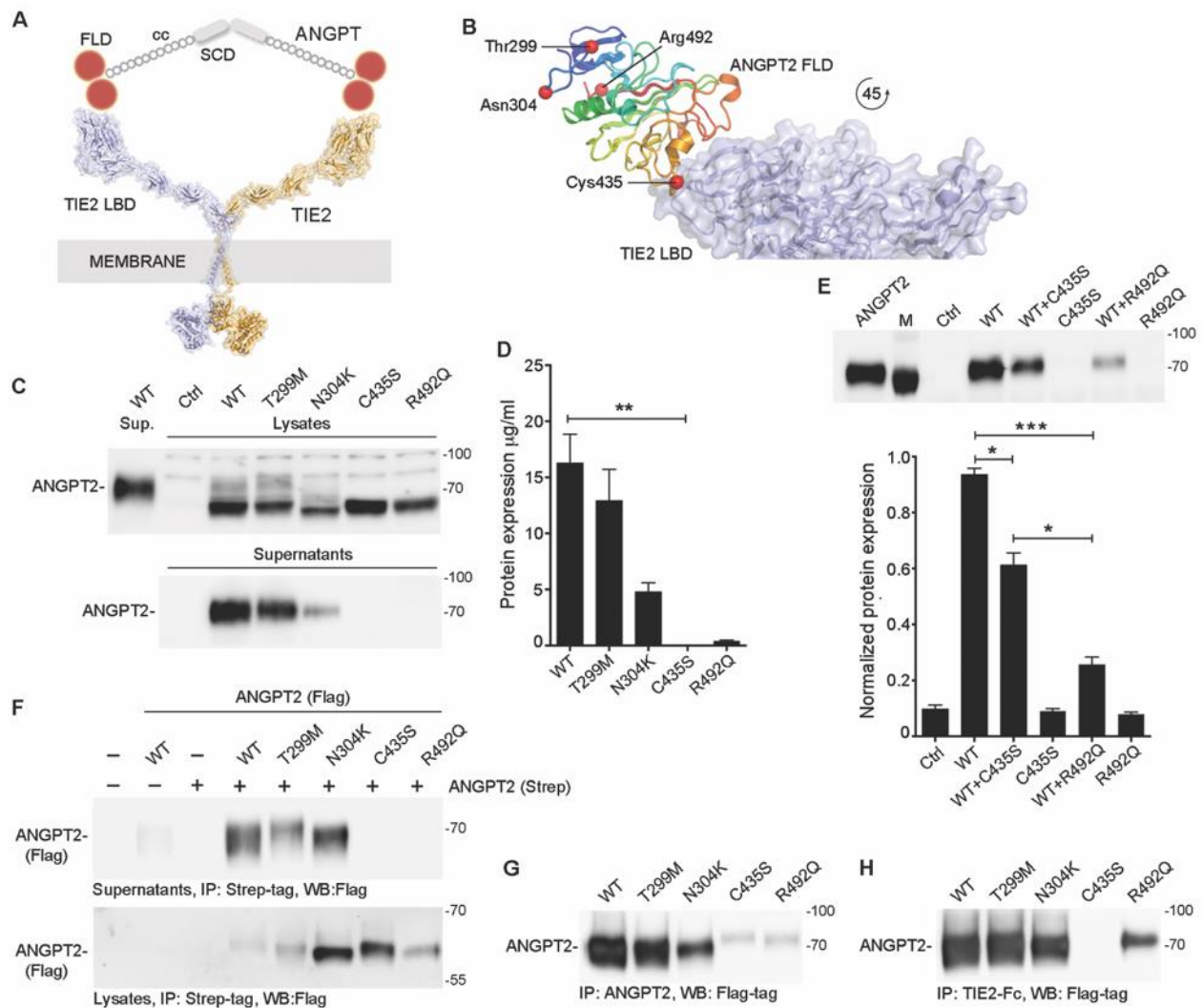
Fig. 2. Expression analysis and TIE2 binding of ANGPT2 mutants. (**A**) A model of tetrameric angiopoietin and TIE2 dimerization. (**B**) Location of the amino acid substitutions in the structure of the ANGPT2-TIE2 complex (PDB code 2GY7). (**C**) Western blot of WT and mutant ANGPT2 transfected HEK293 cell lysates and supernatants under reducing conditions. (**D**) Elisa-based quantification of ANGPT2 expression in *C*. Kruskal-Wallist test. (**E**) Co-expression of WT-ANGPT2 with C435S or R492Q mutant and quantification of total soluble ANGPT2. M, marker. (**F**) Western blot of the Strep-tagged ANGPT2 and Flag-tagged WT and mutant ANGPT2-transfected HEK293 cell supernatant and lysates. (**G** and **H**) Western blot of WT and mutant ANGPT2 precipitated with ANGPT2 antibody or TIE2-Fc, respectively, from transfected HEK293 supernatants. Error bars: SEM. *, $p \le 0.05$; Dunnett's T3 test, n=3.

25
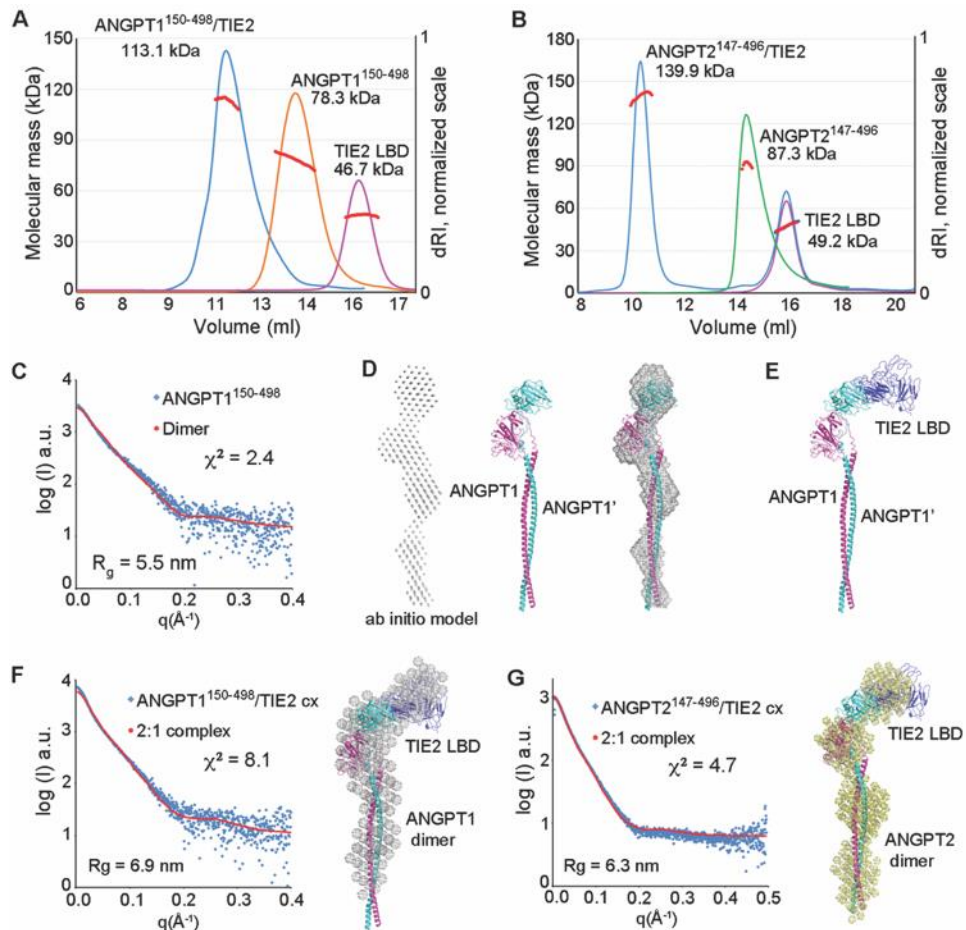
Fig. 3. SEC-MALLS and SAXS analysis of the N-terminally truncated ANGPTs and their complexes with TIE2-LBD. (**A**) SEC-MALLS analysis of ANGPT1[150-498], TIE2-LBD and their complex. Molecular mass (red) and refractive index in arbitrary units (AU) are plotted as a function of elution volume. (**B**) Same as in *A* but for ANGPT2[147-496]. Here the complex was loaded with an excess of TIE2. (**C**) Scattering intensities (I, arbitrary units a.u.) as a function of the scattering vector *q* for ANGPT1[150-498]. (**D**) Ab initio model of ANGPT1[150-498] and comparison with the homology model. (**E**) Model of N-terminally truncated ANGPT in complex with TIE2-LBD. (**F** and **G**) SAXS analysis of the ANGPT1[150-498] and ANGPT2[147-496] complexes with TIE2-LBD, respectively. In (C), (F), and (G), the expected scattering profiles calculated by CRYSOL (*42*) (*43*) from the homology models are superimposed with the observed data, as indicated. Radius of gyration (R_g) is indicated for the scattering data. The ab initio models were calculated with DAMMIF and the homology models were rigid-body refined with SASREF (*43*). χ^2 values indicate the fit of the expected scattering to the scattering data. dRI, differential refractive index; LBD, ligand-binding domain; cx, complex.
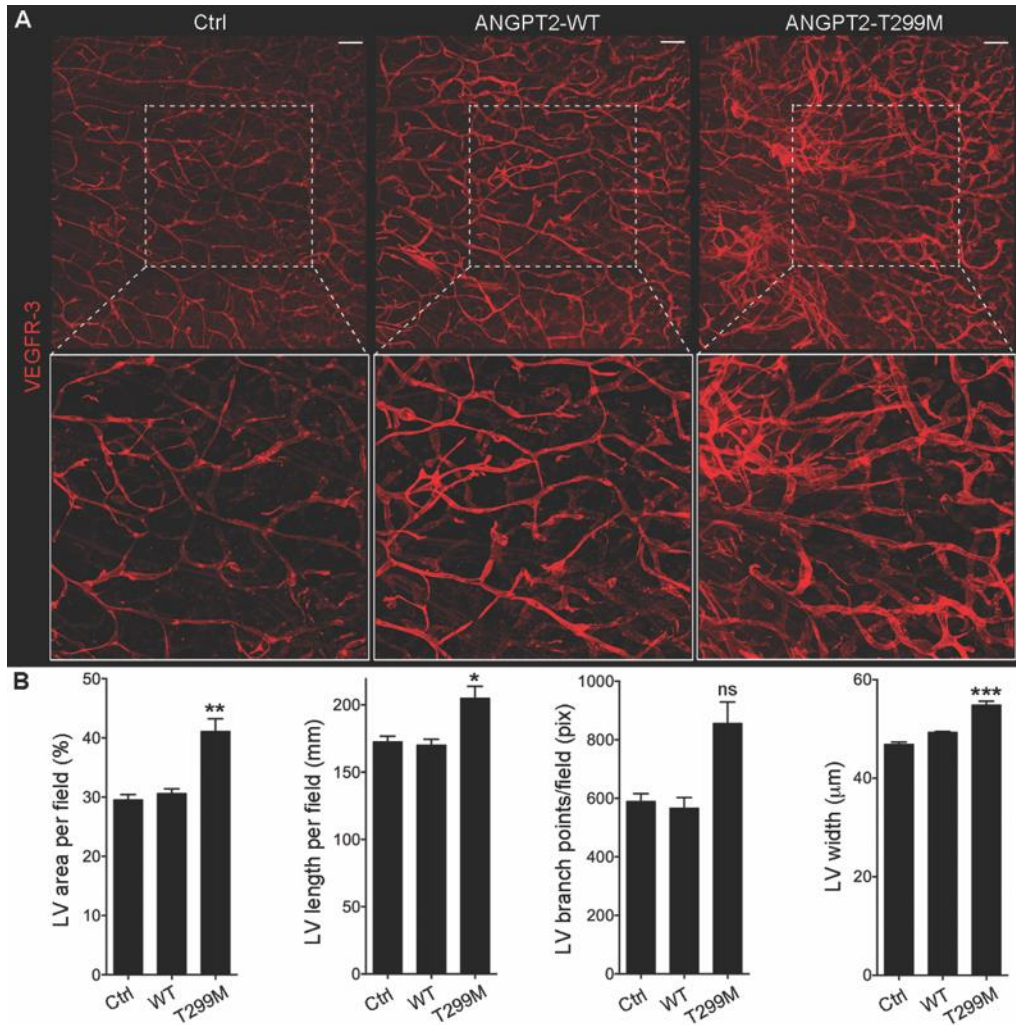
Fig. 4. Effects of the AAV-transfected WT and T299M mutant ANGPT2 on lymphatic vessels in mouse ear skin. (**A**) Representative images of lymphatic vessels (LVs) visualized by VEGFR-3 (red) whole-mount immunofluorescence staining four weeks after transduction with the indicated control (Ctrl), WT, or T299M mutant ANGPT2 AAVs. Scale bars, 200 μm. (**B**) Quantification of LV area, skeleton length, branch points, and width per image field in pixels (pix) using the AutoTube program (*57*). Error bars: SEM. *, $p \leq 0.05$;**, $p \leq 0.01$; ***, $p \leq 0.001$;. Kruskal-Wallis test, n=6.
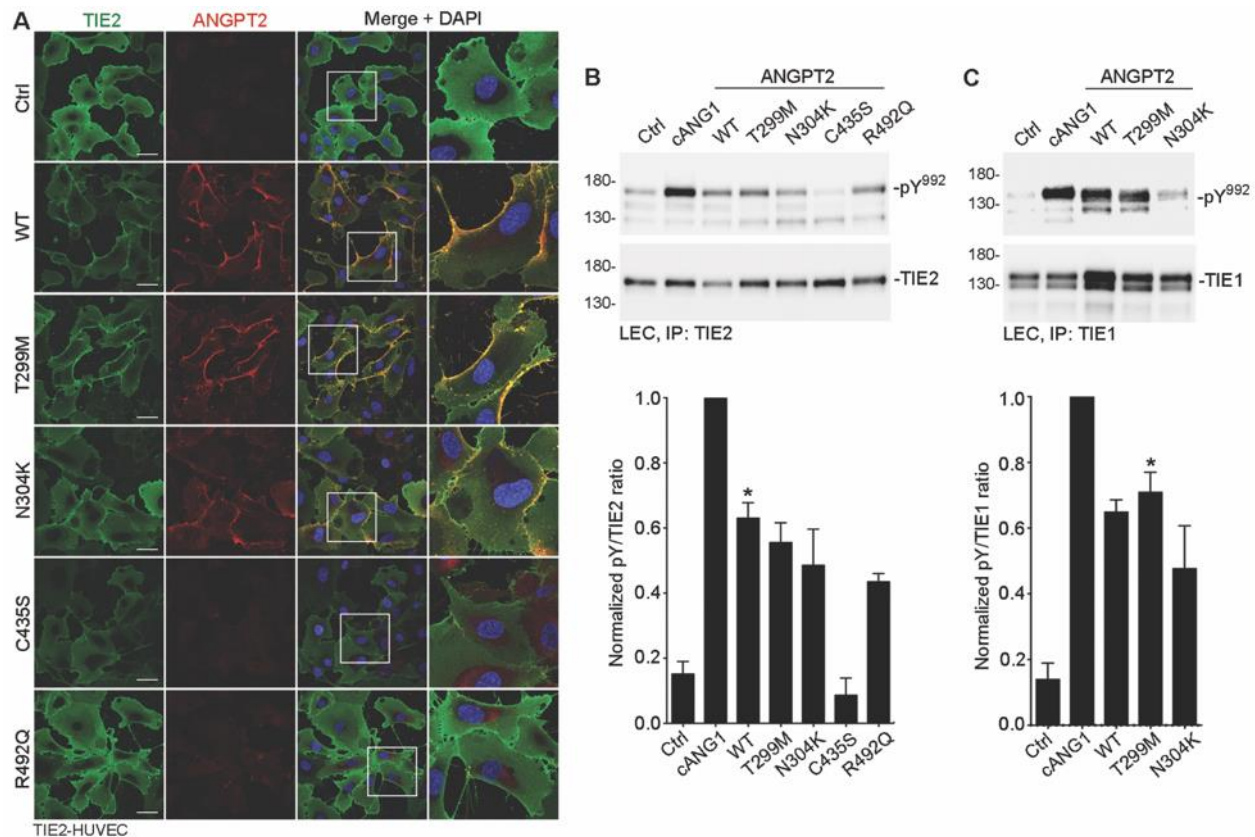
Fig. 5. ANGPT2-induced activation of TIE2 and TIE1. (**A**) ANGPT2 and TIE2 double-transfected HUVECs were stained with anti-Flag (red, ANGPT2) and TIE2 antibodies (green). Cells were not permeabilized and nuclei were stained with DAPI. TIE2-transfected HUVECs were used as ANGPT2-negative controls for imaging (Ctrl). The rightmost panel shows the inset of the merged stainings. Scale bars, 50 μm. (**B**) Western blot of TIE2 phosphorylation in ANGPT2-transfected LECs. Control cells were stimulated with COMP-ANGPT1 (cANG1, 500 ng/ml) for 1 h or left unstimulated (Ctrl). (**C**) Western blot analysis of TIE1 phosphorylation in ANGPT2-transfected LECs. Phospho-Tyr992/total TIE ratios (pY/TIE) were normalized by using COMP-ANGPT1 stimulations and the phospho-Tyr992/total TIE ratios of ANGPT2 stimulations were compared to unstimulated control cells. Error bars: SEM. *, $p \leq 0.05$. Kruskal-Wallis test, n=3 (TIE2), n=4 (TIE1).
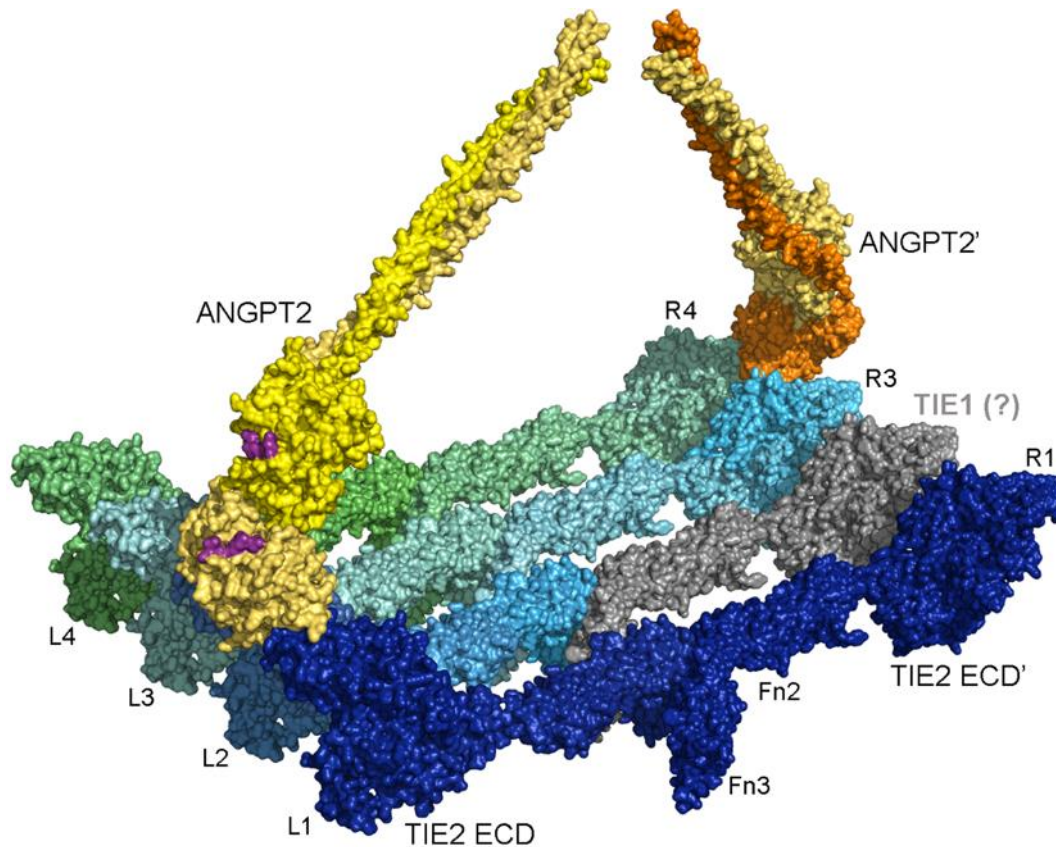
Fig. 6. ANGPT2 tetramer and TIE2 clustering. An array of four TIE2 extracellular domain (ECD) homodimers in a clustering model proposed by (*55*). ANGPT2 dimers (in complex with the TIE2 LBD) are derived from the SAXS data in this manuscript. The models based on SAXS data are here shown with the previously solved crystal structures of Fn2 and Fn3 domain mediated TIE2 dimerization and clustering (*54, 55*). The TIE2 ECDs are labeled on the right side from R1 to R4 and on the left side from L1 to L4. The ANGPT2[147-495] dimers based on the SAXS data are shown as surface models bound to L1 and R4 TIE2 ECDs on the opposite sides. The orphan TIE1 receptor may act as an intervening receptor by the type III fibronectin domain 3 (Fn3) mediated TIE2 heterodimerization (*54, 55*). Integrin-α5 binding sites in ANGPT2 dimer, centered on Gln362 residues (*30*), are highlighted in purple.

Supplementary Materials for

Characterization of ANGPT2 mutations associated with primary lymphedema

Authors: Veli-Matti Leppänen, Pascal Brouillard, Emilia A Korhonen, Tuomas Sipilä, Sawan Kumar Jha, Nicole Revencu, Veerle Labarque, Elodie Fastré, Matthieu Schlögel, Marie Ravoet, Amihood Singer, Claudia Luzzato, Donatella Angelone, Giovanni Crichiutti, Angela D'Elia, Jaakko Kuurne, Harri Elamaa, Gou Young Koh, Pipsa Saharinen, Miikka Vikkula and Kari Alitalo

Materials and Methods

ANGPT2 gene sequencing

To screen the *ANGPT2* gene for mutations, we designed an Ion Ampliseq panel for targeted amplification and sequencing of the nine exons, as well as 10 bp of flanking introns. Sequencing was performed using 10 ng of genomic DNA on an Ion Torrent Personal Genome Machine, according to the recommended protocols (Thermo Fischer Scientific). The reads (average coverage of 132x) were aligned to the Human reference genome hg19, and imported in Highlander, a NGS data analysis software developed in Brussels (http://sites.uclouvain.be/highlander/), for variant calling and annotation. Variant filtering was set to keep only variants predicted damaging by at least three software programs out of eight used (CADD, Deogen, FATHMM, LRT, Mutation assessor, MutationTaster, Polyphen2, and SIFT) and reported at a frequency less than 0.15% in ExAC (http://exac.broadinstitute.org/), the estimated frequency of primary lymphedema in the general population. Frequencies were also checked to be below 0.15% in gnomAD (https://gnomad.broadinstitute.org/) a larger genomic database that also contains ExAC data. Validation of the selected changes and co-segregation analyses were performed using Sanger sequencing, with primers designed in introns to amplify the exons containing the changes.

Protein expression and purification

Human ANGPT1 residues 150-498 (ANGPT1$^{150\text{-}498}$) and 245-498 (ANGPT1$^{245\text{-}498}$) and human and mouse TIE2 residues 1-443 (TIE2 LBD) were cloned into the pFastBac (Invitrogen) baculovirus expression vector with a C-terminal His-tag. The ECD of α5 subunit of human α5β1 integrin (residues 42-993) were cloned to the same vector with a C-terminal Fc-tag. Recombinant baculovirus was produced in Sf9 insect cells in serum-free Insect-Express (Lonza) medium supplemented with 50 μg/ml gentamycin (Sigma) at 26 °C. For protein expression, Tn5 insect cells were infected with the corresponding recombinant baculovirus at high multiplicity and at three days post-infection, the supernatant was harvested by centrifugation. Human ANGPT2 residues

147-496 (ANGPT2$^{147-496}$) were cloned into the pLenti-CMV-Puro mammalian cell expression vector with a C-terminal Strep-tag. For ANGPT2$^{147-496}$ protein expression, HEK293 cells maintained in DMEM (Lonza) supplemented with 10% FBS were plasmid transfected with Lipofectamine PLUS (Invitrogen). The secreted ANGPT2$^{147-496}$ in culture media was purified by column chromatography with streptactin sepharose affinity resin (IBA) and eluted with D-desthiobiotin (Sigma-Aldrich). The His-tagged proteins were extracted by Ni^{2+}-charged chelating sepharose (GE Healthcare), the resin was washed in PBS containing 20 mM imidazole and the proteins eluted with 0.4 M imidazole in PBS. Finally, the proteins were purified by gel filtration on a Superdex 200 (GE Healthcare) column in 10 mM HEPES, 0.15 M NaCl at pH 7.4 (HBS, hepes buffered saline). ANGPT1$^{150-498}$ and its complex with TIE2 LBD were purified similarly in a buffer with higher NaCl concentration (300 mM) and supplemented with 50 mM imidazole.

The human lymphedema patient ANGPT2 mutants (T299M, N304K, C435S and R492Q) and the WT control protein were cloned into pFUW lentivirus vector (Addgene plasmid #14882) with a C-terminal Flag-tag. The proteins were expressed in HEK293 cells in DMEM (Lonza) supplemented with 10% FBS, and the secreted recombinant proteins in culture media were purified by column chromatography with M2 anti-Flag affinity resin (Sigma-Aldrich) and eluted with 0.1 M Glycine (pH 3.5) that was immediately neutralized with pH 8 Tris buffer.

SAXS data collection and analysis

The ANGPT1$^{150-498}$ and CA1-3 complexes with TIE2 LBD were formed by mixing the proteins in a molar excess of TIE2 LBD in 300 mM NaCl, 50 mM Imidazole and 20 mM Hepes (pH 7.4). The ANGPT2$^{147-496}$ complexes with TIE2 LBD were formed similarly without Imidazole and NaCl at 150 mM. The complexes were purified by size-exclusion chromatography column (Superdex 200; GE Healthcare) in the same buffer with 5% glycerol. The protein samples for SAXS were concentrated by using Amicon Ultra-4 centrifugal filter units (EMD Millipore) and frozen for storage at -80°C. The size-exclusion chromatography column buffer was used as a solvent blank for SAXS.

SAXS data were collected on the beamline BM29 at ESRF (Grenoble, France). Each sample had 10 exposures taken at a sample-to-detector distance of 2.867 m and at 12.5 keV, covering a

momentum transfer q-range of 0.0025 - 0.5 Å^{-1}. Samples were continuously passed through the beam using a flow through capillary cell to minimize radiation damage. The 10 consecutive exposures were compared for change in scattering intensity due to radiation damage. Radially averaged scattering data were buffer subtracted and analyzed by using ATSAS (2.8.1) software (42). Scattering curves were displayed as the scattering intensity ($I(q)$) as a function of momentum transfer $q = (4\pi\sin\theta)/\lambda$, where λ is the wavelength of the incident X-ray beam and θ is half the angle between the incident and scattering radiation. SAXS data were obtained in at least three different concentrations and the data was checked for aggregation by examination of the linearity in the Guinier region in log ($I(q)$) versus log (q) plots, a diagnostic of sample quality.

The R_g (radius of gyration) was calculated from the scattering curve by using the indirect Fourier transform program AUTOGNOM, which additionally provides an estimate of the maximum particle dimension (D_{max}) from the distance distribution function $P(r)$. AUTOGNOM was also used to assign the q range for ab initio shape reconstructions by DAMMIF, which uses simulated annealing methods to build low resolution protein models from densely packed beads inside a search volume. The final model was obtained by aligning ten independent models to produce an averaged, volume-filtered model. Experimental scattering curves were compared with theoretical scattering curves calculated by the program CRYSOL (for q_{max}<0.5 Å^{-1}) from the homology models based on Fibrinogen beta and gamma chains and the ANGPT1-TIE2 complex structures.

Multi-angle laser light scattering

SEC-MALLS measurements were run in a Superdex 200 10/300 column (GE Healtcare) in HBS with a Shimadzu HPLC system and MiniDAWN TREOS light scattering detector and Optilab rEX refractive index detector (Wyatt Technology Corporation). Samples were loaded at about 50 µM concentrations and, considering about a 20-fold dilution in column chromatography, the light scattering was measured at about 1-3 µM concentrations. The ANGPT1[150-498] samples were run with 300 mM NaCl and 50 mM imidazole. Data were analyzed with ASTRA 6 software (Wyatt Technology Corporation).

Binding assays

For Surface Plasmon Resonance (SPR) with Biacore T100, TIE2-Fc (R&D Systems) was immobilized to a C1 chip (GE-Healthcare) using a direct immobilization program to achieve a final response of 340 RUs. As a control, TIE1-Fc was immobilized to a control well using an automated immobilization program (400 RU). ANGPT2-FLD-Fc or ANGPT2-FLD-Fc with T299M or N304K substitutions, all in HBS-P buffer (GE-Healthcare), were applied as analytes onto the chips, at a flowrate of 10 µl/min for total of 300 s. For each protein a concentration gradient from 2.5 to 40 µg/ml was used. The chip was washed with 1 M MgCl after each injection. Fc-tagged TIE2 LBD binding to the full-length T299M or N304K mutant or WT-ANGPT2 was measured with an Elisa assay. ANGPT2 concentrations in HEK293 supernatants were measured by ANGPT2 ELISA kit (DuoSet, R&D Systems).

Cell culture and lentiviral generation
HEK293 cells were maintained in Dulbecco's modified Eagle's medium (DMEM, Lonza) supplemented with 2 mM L-glutamine, penicillin (100 U ml^{-1}), streptomycin (100 µg ml^{-1}) and 10% FBS. HUVECs and LECs (PromoCell) were grown in Endothelial Cell Basal Medium MV (ECBM) supplemented with Supplement Pack GM MV (PromoCell) on gelatin-coated (0.1%) culture plates or coverslips. Lentivirus packaging cell line 293FT was maintained in DMEM (Lonza) with 4.5 g/L glucose and supplemented with 10% FBS, 1% L-glutamine, 0.2% penicillin, 0.2% streptomycin, 0.2% puromycin, 0.6% neomycin and 1 µg/ml tetracycline. The 293FT cells were transformed with FUW lentiviral expression vectors with Fugene 6 (Roche) in DMEM supplemented with 4,5g/l glucose, 10% FBS, 1% glutamine, 0.2% penicillin and 0.2% streptomycin. Media were chanced after 48 and 72 h and the lentiviruses were concentrated by overnight centrifugation at 6800xg, +4.

Phosphorylation of TIE2 and TIE1
For paracrine TIE2 activation, human endothelial cells were starved for 2-3 h in 1% FBS containing media, followed by 1 h stimulation with COMP-ANGPT1 as indicated. For autocrine TIE activation, human endothelial cells were transduced at 70-90% confluence by using concentrated lentivirus, medium changed after 48 hours and the cell lysates collected after 72 hours. The cells were lysed, as described previously in 1% Triton-100 containing PLCLB lysis buffer (51) followed by measurement of protein concentration and immunoprecipitation using anti-TIE2 (AF313, R&D

Systems) or anti-TIE1 (AF619, R&D Systems) antibodies and protein G-Sepharose (GE Healthsciences Ab) at +4. Protein concentration of the lysates was measured using the Pierce BCA Protein Assay kit (Thermo Scientific). The immunocomplexes were separated in SDS-PAGE (Bio-Rad Laboratories), transferred to PVDF membrane (Millipore) using the Trans-Blot Turbo Transfer System (Bio-Rad Laboratories). Membranes were used for immunoblotting with anti-phospho-TIE2 (pY-992, AF2720, R&D Systems), anti-TIE1 (AF619, R&D Systems) or anti-TIE2 (AF313, R&D Systems) as primary antibodies and HRP-conjugated secondary antibodies (Dako) or biotinylated secondary antibodies (Dako) followed by ECL detection with the SuperSignal West Pico Chemiluminescent Substrate or SuperSignal West Femto Maximum Sensitivity Substrate (Thermo Scientific). Western blots were imaged with Odyssey FC (LI-COR). For reprobing, the membranes were stripped using the ReBlot Plus Strong Antibody stripping buffer (Millipore). Western blots were quantified using ImageJ.

AAV-mediated *ANGPT2* gene transfer

4×10^{10} PFUs/mouse of empty control or the T299M mutant or the WT-ANGPT2 coding AAV vector in 40 μl of PBS were injected into six-week old mice ear skin. Four weeks later, the mice were sacrificed and the dorsal sides of the ears were collected for whole mount VEGFR-3 immunofluorescence staining as in (*23*). Fluorescently labeled whole mount samples were imaged using a Zeiss LSM 880 confocal microscope (air objective 10× Plan-Apochromat with NA 0.45) and processed with Fiji ImageJ.

Immunofluorescence imaging

For immunofluorescence staining of TIE2- and ANGPT2-transfected HUVECs, the cells were fixed with 4% PFA, permeabilized with 0.1% Triton-X100 or left unpermeabilized and stained using anti-TIE2 (AF313, R&D Systems) or anti-Flag antibodies together with Alexa-conjugated secondary antibodies (Life Technologies). The samples were mounted with Vectashield mounting medium containing DAPI (Vector Labs). Images were captured with a Hamamatsu digital camera (ORCA-Flash4.0 LT) connected to a Zeiss Axio Imager 2 epifluorescence microscope.
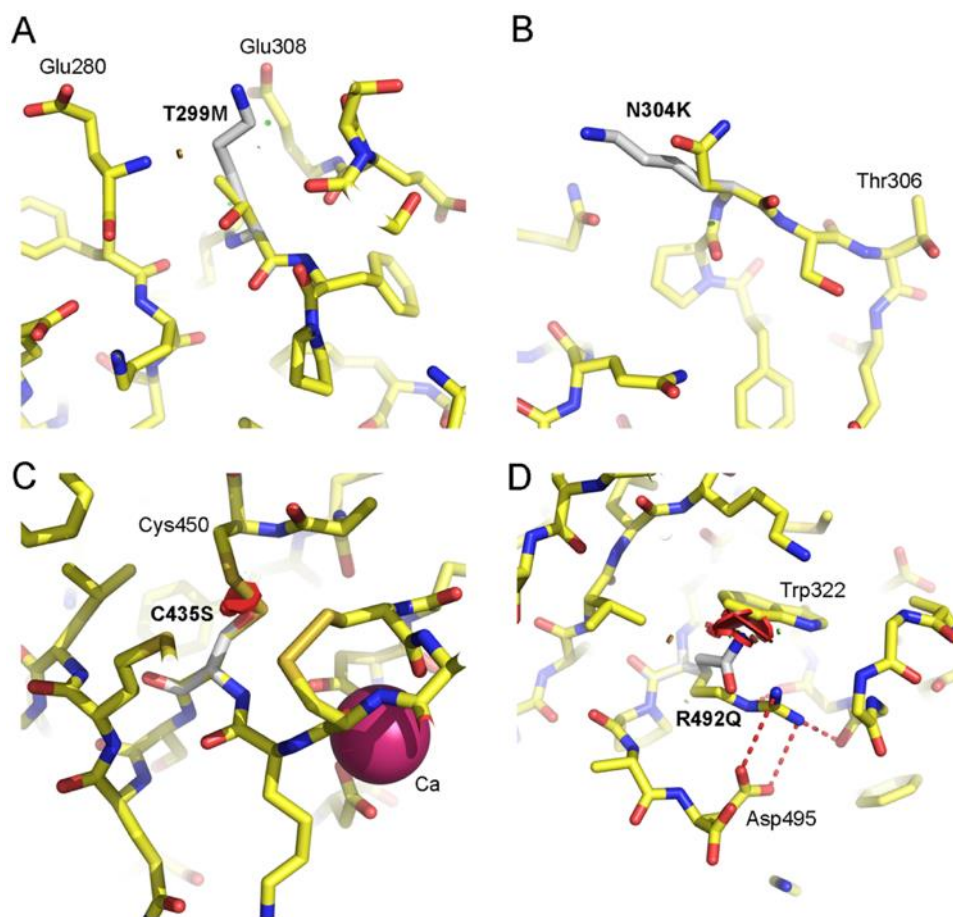
Fig. S1. Structural characterization of ANGPT2 mutations. Close-ups of the effects of T299M (**A**), N304K (**B**), C435S (**C**), and R492Q (**D**) mutations, respectively, on ANGPT2 structure and interactions with the neighboring residues. Unfavorable van der Waals interactions and steric clashing with the neighboring residues as shown by the red discs.
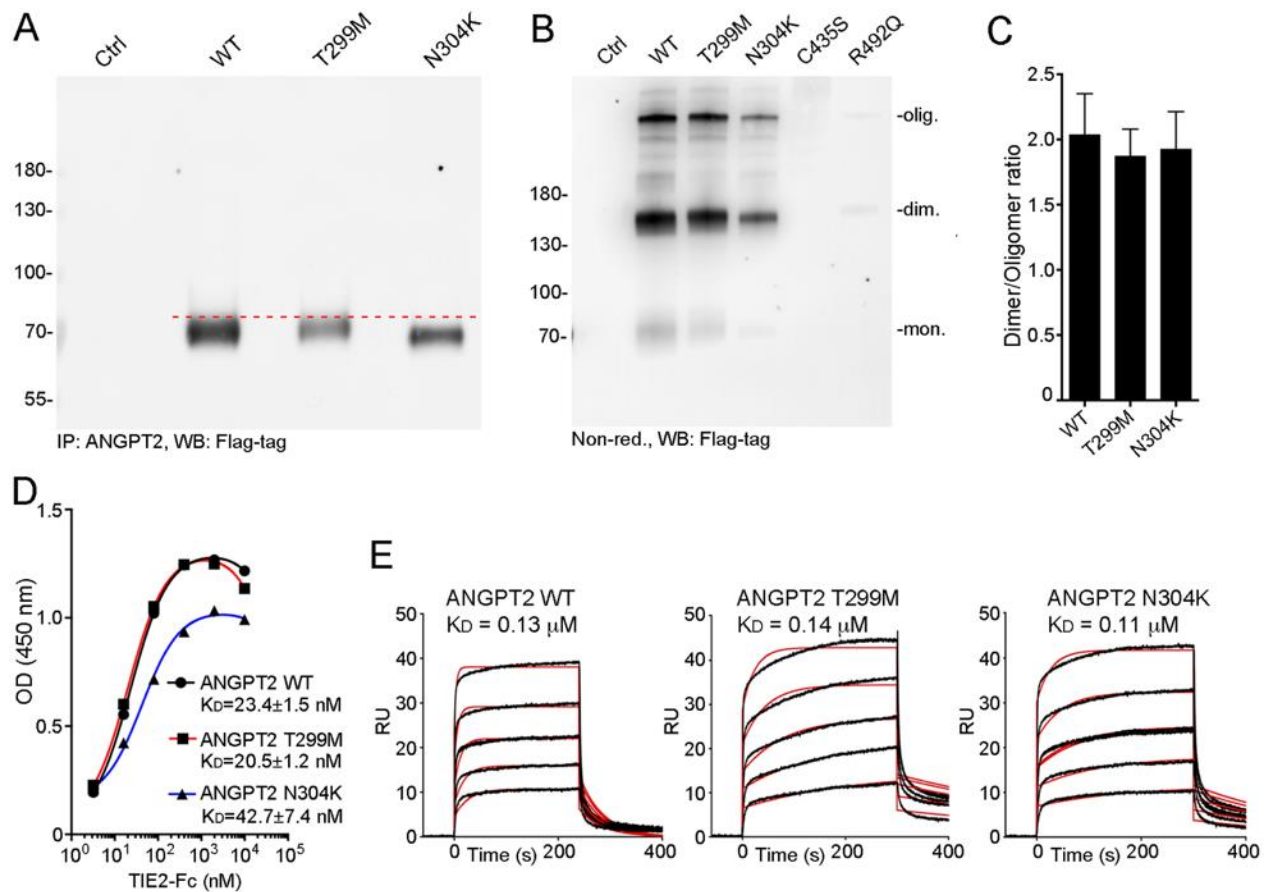
Fig. S2. Characterization of the oligomerization and TIE2 binding of ANGPT2 mutants. (A) Western blot analysis of the T299M and N304K mutants and WT-ANGPT2-transfected HUVEC supernatants under reducing conditions. A dashed line marks the trailing edges of the T299M mutant and WT-ANGPT2 and shows the smaller molecular weight of the N304K mutant ANGPT2 polypeptide. (**B**) Western blot analysis of the T299M and N304K mutants under nonreducing conditions. (**C**) Quantification of the dimer to oligomer ratios in *B*. Error bars: SEM. Kruskal-Wallis test, n=4. (**D**) A linear regression analysis of TIE2-Fc binding to the T299M and N304K mutants and to WT-ANGPT2. (**E**) Surface plasmon resonance binding assays of TIE2-Fc and ANGPT2 mutants. Binding curves (black) and simulation results (red) are shown.
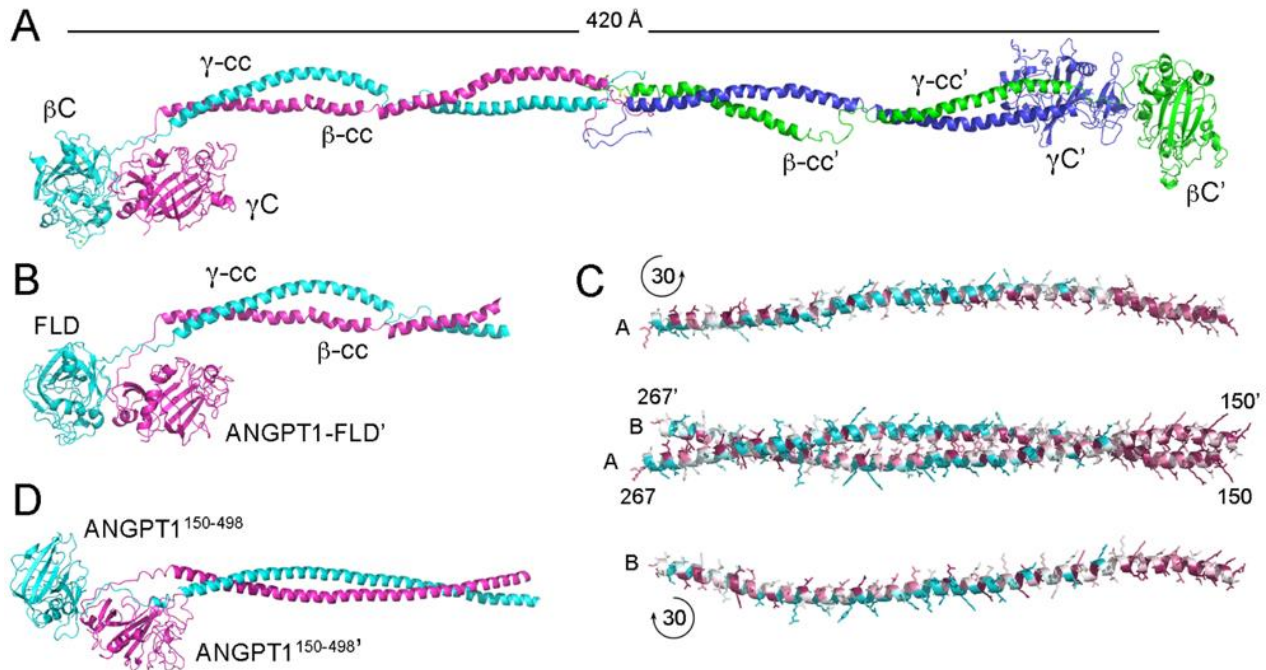
Fig. S3. A fibrinogen-based homology model of dimeric ANGPT1$^{150-498}$. (**A**) Crystal structure of human fibrinogen tetramer of β- and γ-chains as a cartoon model (PBD code 3GHG). Note the distance between the βC domains in the tetramer. The α-chains lacking C-terminal fibrinogen-like domains were omitted from the figure. Fibrinogen oligomerization is based on intermolecular disulfide bridges in the N-terminal domain. (**B**) An intermediate model where the ANGPT1 fibrinogen-like domain from the PDB entry 4K0V was superimposed with the fibrinogen C-terminal domains, and the length of the coiled-coil domains was shortened. (**C**) A homology model of the dimeric ANGPT1 coiled-coil domain of residues 150-267. The model was generated by the Phyre2 program and it is based on keratin heterodimer (PBD code 4ZRY). The cartoon/stick model shows residues colored according to the rate of evolutionary conservation, from cyan to magenta. The A and B chains are shown also separately to better visualize the stripe of conserved residues forming the hydrophobic inner layer of the coiled coils. (**D**) The final homology model of dimeric ANGPT1$^{150-498}$ with the fibrinogen coiled-coil domains replaced with the homology model based on a keratin heterodimer.
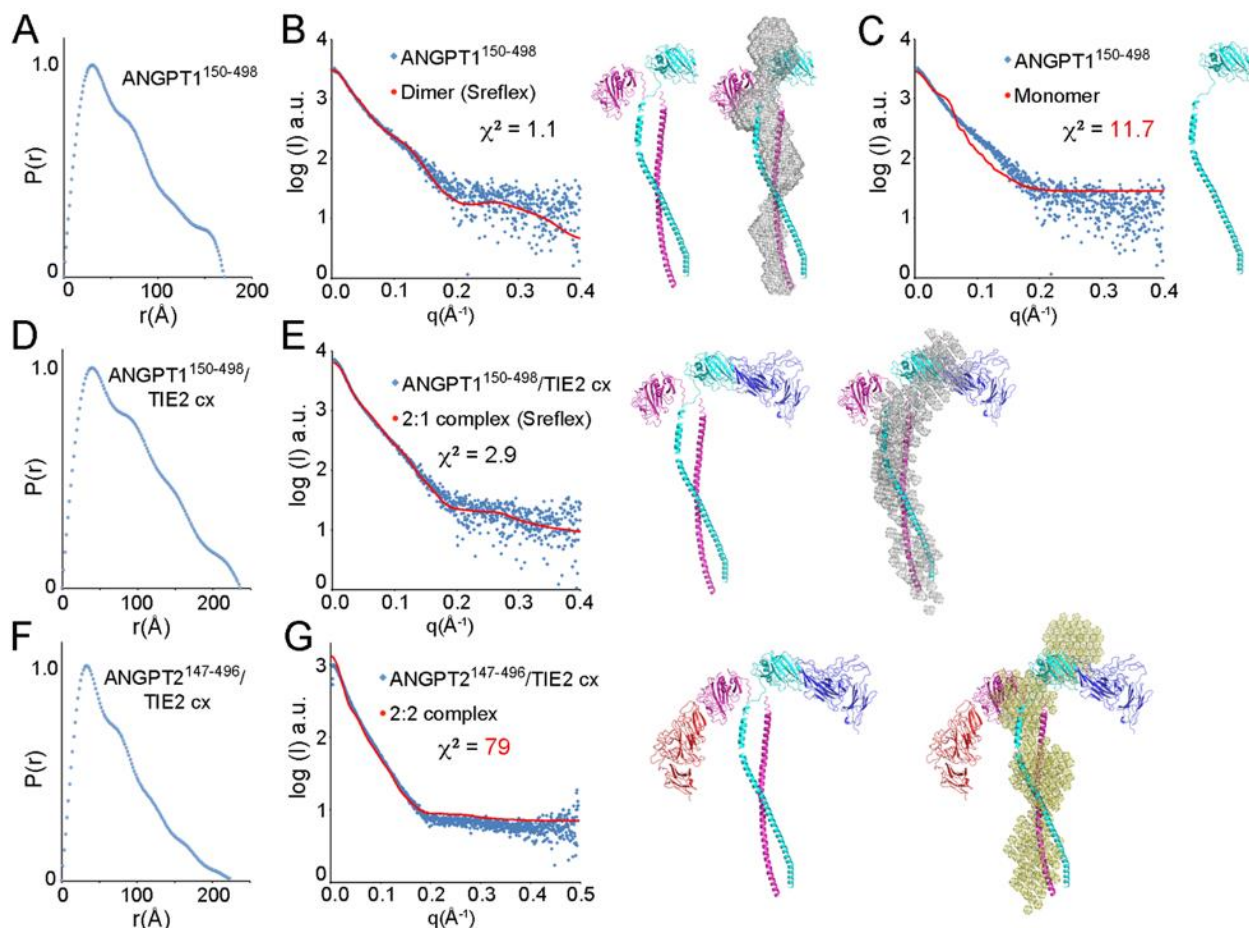
Fig. S4. SAXS analysis of the N-terminally truncated ANGPT1[150-498] and ANGPT2[147-496]. (**A**) Normalized pair distance distribution function (*P(r)*) for ANGPT1[150-498]. (**B**) Scattering profile and scattering intensities (I, arbitrary units a.u.) as a function of the scattering vector *q* for ANGPT1[150-498] and the expected scattering profile (red line) from the SREFLEX-refined (41) homology model. The refined homology model is shown in cartoon with and without the comparison to the representative ab initio 3D model shown in mesh. (**C**) Comparison of the expected scattering profile of a monomeric ANGPT1[150-498] to the scattering data. (**D** and **E**) SAXS analysis of the ANGPT1[150-498]/TIE2 complex as in (A) and (B). The SREFLEX-refined homology model is shown in cartoon with and without the comparison to the representative ab initio 3D model shown in mesh. (**F** and **G**) SAXS analysis of the ANGPT2[147-496]-TIE2 complex as in *A* and *B*. A SREFLEX-refined homology model in 2:2 stoichiometry is shown in cartoon with and without the comparison to the representative ab initio 3D model shown in mesh. The χ^2 values indicate the fit of the expected scattering to the scattering data.
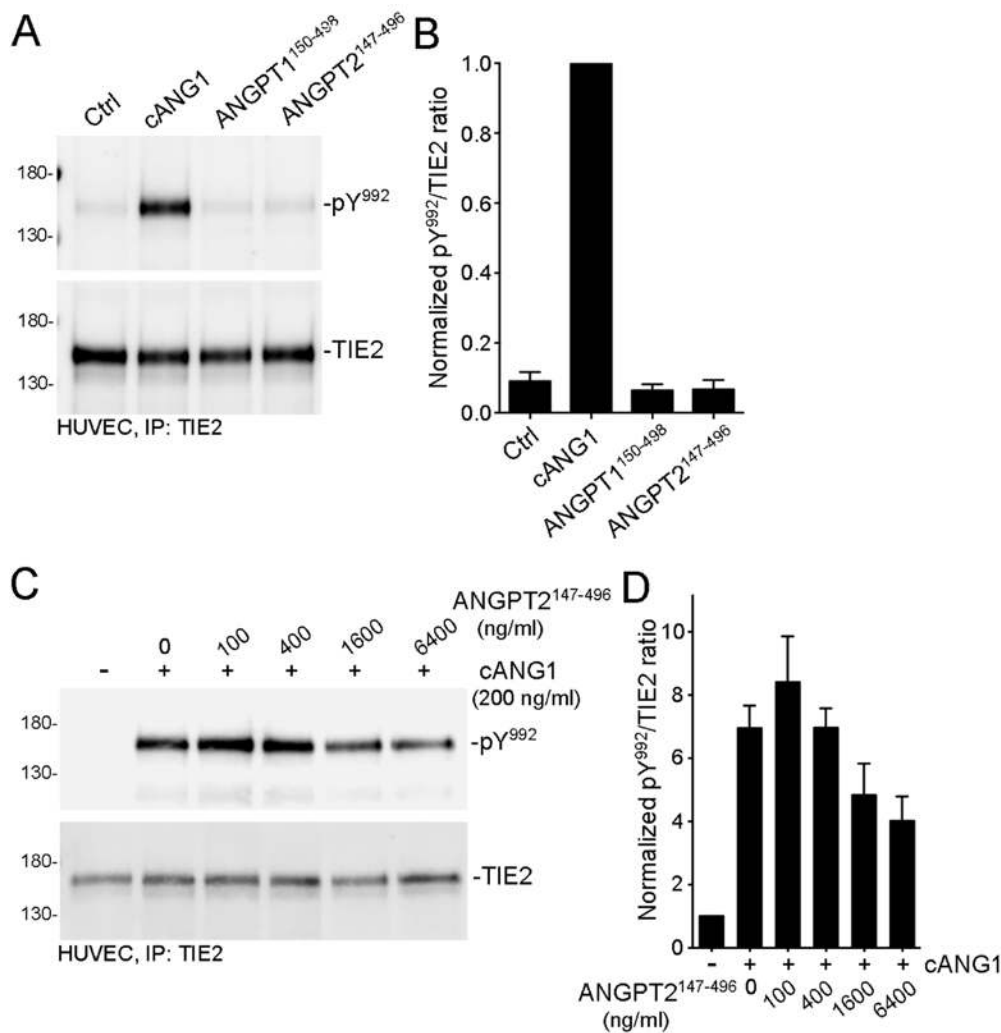
Fig. S5. Dimeric angiopoietins are TIE2 antagonists. (**A**) Western blot analysis of TIE2 phosphorylation in HUVECs. Cells were stimulated with COMP-ANGPT1 (cANG1), ANGPT1[150-498] and ANGPT2[147-496] at 500 ng/ml for 1 h or left unstimulated. (**B**) Quantification of normalized Phospho-Tyr992(pY992)/total TIE2 ratios in (A) (Krushkal-Wallis's test, n=3). (**C**) Western blot analysis of TIE2 phosphorylation in HUVECs in a competition assay of COMP-ANGPT1 stimulation (200 ng/ml, 1h) with increasing concentrations of the dimeric ANGPT2[147-496]. (**D**) Quantification of normalized Phospho-Tyr992/total TIE2 ratios in (C) (Krushkal-Wallis's test, n=3). Error bars: SEM.
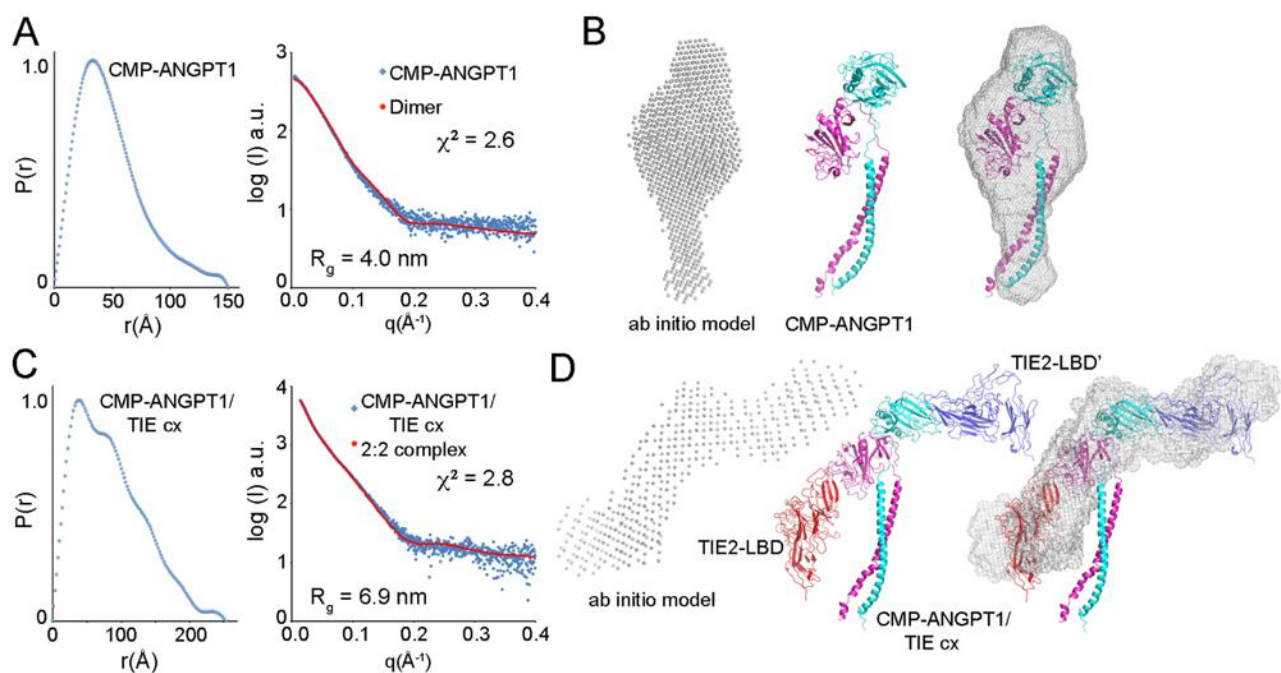
Fig. S6. SAXS analysis of the dimeric CMP-ANGPT1 and its complex with TIE2 ligand-binding domain. (**A** and **C**) Normalized pair distance distribution functions (*P(r)*) and scattering profiles and scattering intensities (I, arbitrary units a.u.) as a function of the scattering vector *q* for dimeric CMP-ANGPT1 (44) and its complex with TIE2 ligand-binding domain, respectively, and the expected scattering profiles (red lines) from the homology models. Radius of gyration (R_g) is indicated for the scattering data, and the ab initio models were calculated with DAMMIF and the homology models were rigid-body refined with SASREF (42). The χ^2 values next to refined models indicate the fit of their expected scattering to the scattering data. (**B** and **D**) Comparison of the representative ab initio 3D models shown in spheres and in mesh with the SASREF-refined homology models shown in cartoon. LBD, ligand-binding domain; cx, complex.
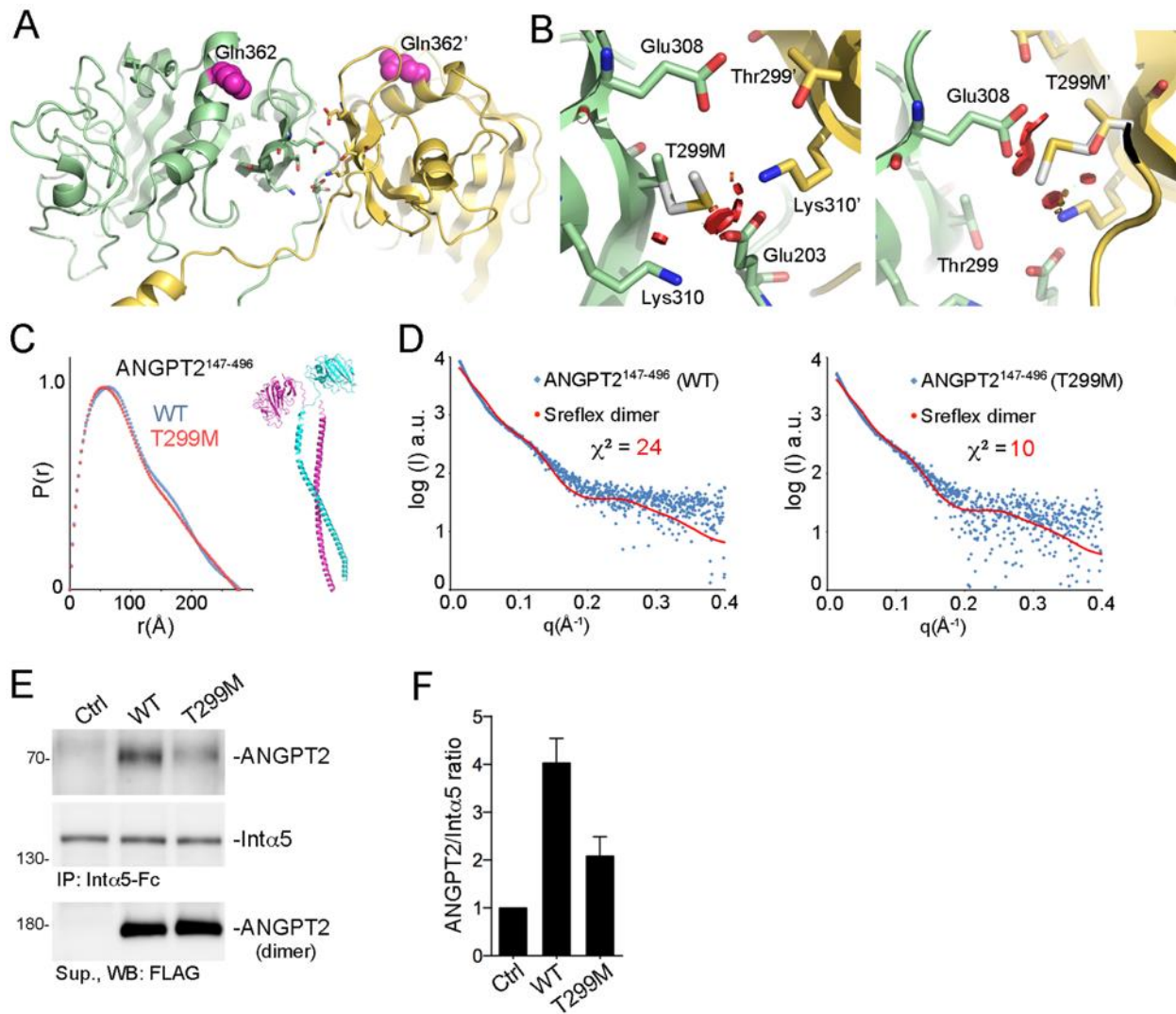
Fig. S7. The T299M mutation is located in the dimerization interface of ANGPT2 fibrinogen-like domains and shows decreased integrin-α5 binding. (**A**) Interactions in the dimerization interface of the ANGPT2 homology model and SAXS analysis of the WT and T299M mutant of ANGPT2$^{147-496}$. Thr299 is located in the Gln362-centered integrin-α5 subunit binding sites are highlighted in magenta. (**B**) Close-ups of (A) centered on Thr299 and Thr299'. The larger methionine sidechains in the T299M mutant may induce steric clashes in the dimerization interface, as indicated by the red discs. (**C**) Normalized pair distance distribution functions (*P(r)*) of the SAXS analysis of the WT and the T299M mutant of ANGPT2$^{147-496}$ and a N-terminally truncated ANGPT homology model shown in fig. S4B. (**D**) Scattering profile and scattering intensities (I, arbitrary units a.u.) as a function of the scattering vector *q* for the WT and the T299M mutant of ANGPT2$^{147-496}$, and the expected scattering profile (red line) from the SREFLEX-refined

homology model. (**E**) Representative western blot analysis of the WT and the T299M mutant ANGPT2 precipitated with Fc-tagged integrin-α5 ECD (Intα5-ECD), and straight western blot analysis of the WT and mutant ANGPT2 transfected HUVEC supernatants (Sup.). The gel was run under nonreducing conditions. (**F**) Statistical analysis of WT and T299M mutant ANGPT2 binding to the Intα5-ECD. Error bars: SEM. Mann–Whitney test, n=3.
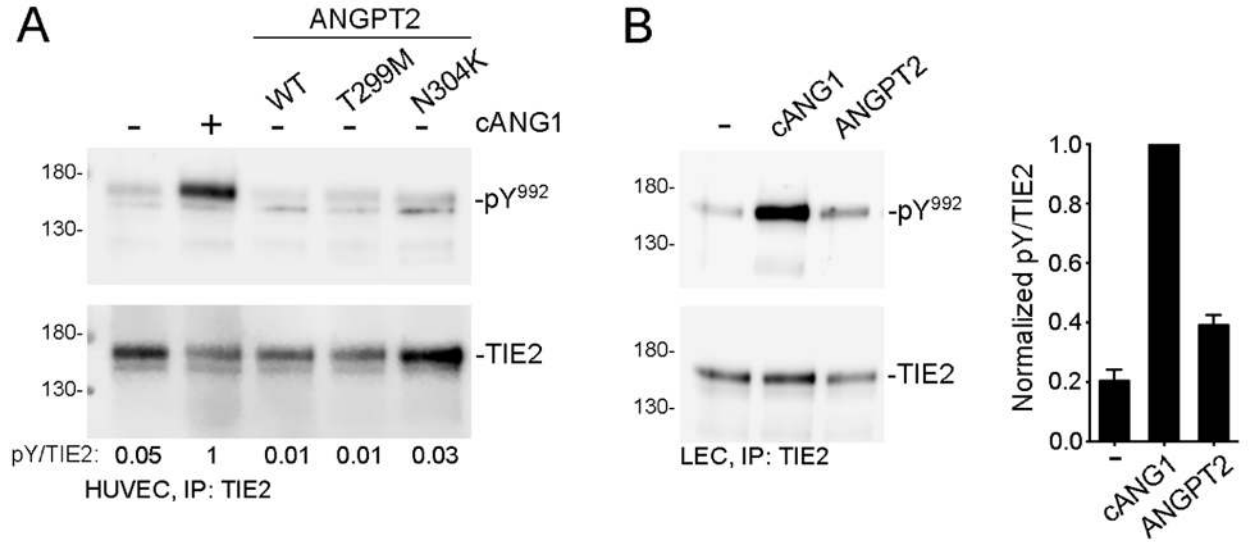
Fig. S8. Paracrine ANGPT2 is a TIE2 antagonist in HUVECs, but a weak agonist in LECs.
(**A**) Western blot analysis of TIE2 phosphorylation in HUVECs. Cells were stimulated with the T299M and N304K mutants of ANGPT2, WT-ANGPT2 or COMP-ANGPT1 (cANG1) at 500 ng/ml for 1 h or left unstimulated. (**B**) A representative Western blot analysis and quantification of LEC stimulations with cANG1 at 500 ng/ml and ANGPT2 at 1000 ng/ml for 1h. The phospho-Tyr992/total TIE2 ratios (pY/TIE2) from ANGPT2 stimulations were compared with the pY/TIE2 ratios of unstimulated control samples after the ratios were normalized with those of cANG1 stimulations. Error bars: SEM. Mann–Whitney test, n=3.
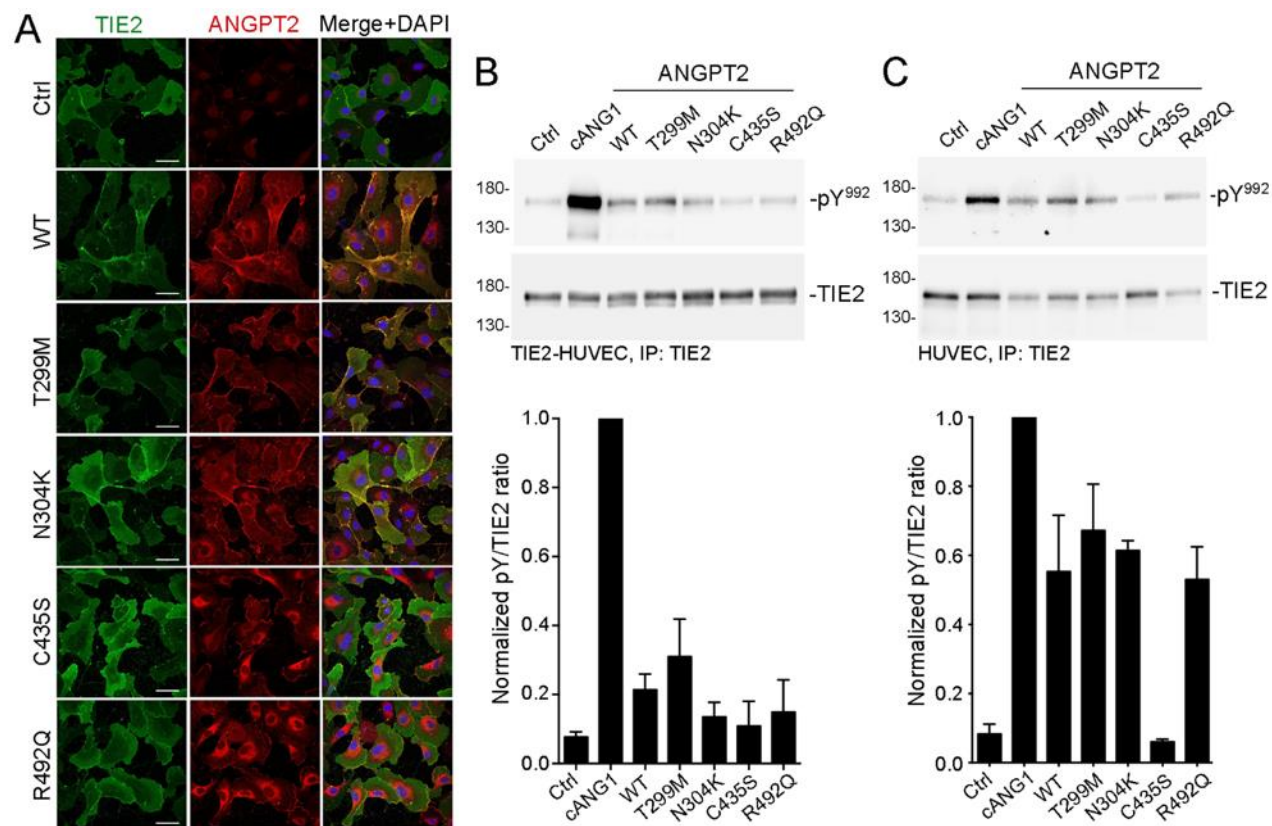
Fig. S9. **ANGPT2 expression and ANGPT2-induced TIE2 activation in HUVECs. (A)** Permeabilized ANGPT2 and TIE2 double-transfected HUVECs were stained with anti-Flag (red) and TIE2 antibodies (green). Nuclei were stained with DAPI. Cells transfected with empty vectors were used as a mock negative control for imaging. Scale bars, 50 μm. **(B)** Western blot analysis of TIE2 phosphorylation in the TIE2 and ANGPT2 double-transfected HUVECs. The TIE2-transfected control cells were stimulated with COMP-ANGPT1 (cANG1) for 1 h or left unstimulated (Ctrl). (**C**) Western blot analysis of TIE2 phosphorylation in the ANGPT2-transfected HUVECs as in *B*. Phospho-Tyr992/total TIE2 ratios (pY/TIE2) were normalized by using COMP-ANGPT1 stimulations. Error bars: SEM. Kruskal-Wallis test, n=3.
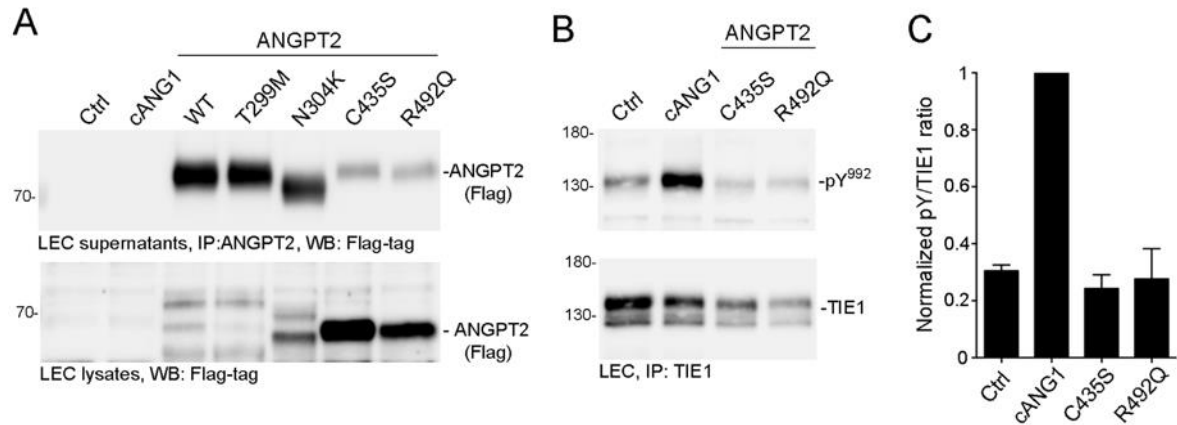
Fig. S10. **ANGPT2 expression and ANGPT2-induced TIE1 activation in LECs. (A)** Western blot analysis of LEC supernatants and lysates from ANGPT2 stimulation in Fig. 5B. **(B)** Western blot analysis of TIE1 phosphorylation in the C435S and R492Q mutant ANGPT2-transfected LECs. The control cells were stimulated with COMP-ANGPT1 (cANG1, 500 ng/ml) for 1 h or left unstimulated (Ctrl). **(C)** Quantification of western blot analysis of TIE1 phosphorylation in *B*. Phospho-Tyr992/total TIE1 ratios (pY/TIE1) were normalized by using COMP-ANGPT1 stimulations. Error bars: SEM. Kruskal-Wallis test; n=3.

Table S1. Summary of the functional impact of the mutations found in patients with PLE.

ANGPT2 mutations	T299M	N304K	C435S	R492Q	Whole-gene
Zygocity	Het	Het	Het	Het	Het
Penetrance	full (n=2)	1 carrier	full (n=2)	1 carrier	de novo
Expression in vitro	normal	normal reduced N-glyc	normal	normal	-
Secretion	normal	reduced	not secreted	very weak	-
Effect on WT secretion	-	partial reduction (co-IP)	dominant-negative	dominant-negative	-
Oligomerization	normal	normal	-	-	-
Binding to TIE2	normal	normal	no	normal, but weak	-
Binding to ITGA5	50% reduced	-	-	-	-
Paracrine TIE2 activation HUVECs	not more than WT	not more than WT	not more than WT	not more than WT	-
Autocrine TIE2 activation in LECs	Yes	Yes	No	Yes	-
Autocrine TIE1 activation in LECs	Yes	weak	No	No	-
Global effect	Lymphangiogenic Altered ITGA5 binding	LOF + DN	LOF + DN	LOF + DN	Haplo-insufficiency

Het, heterozygous; WT, wild-type; LECs, lymphatic endothelial cells; LOF, loss of function; DN, dominant negative